Use of Fish Tracking Data to Model Striped Bass Turbine Encounter Probability in Minas Passage

FINAL REPORT
September 2016

Submitted by
Anna Redden and Brian Sanderson
Acadia University

to the

Offshore Energy Research Association (OERA)
of Nova Scotia

ACER Technical Report No. 122

Citation:

Sanderson, B. and A.M. Redden. 2016. Use of fish tracking data to model striped bass turbine encounter probability in Minas Passage. Final Report to the Offshore Energy Research Association of Nova Scotia. ACER Technical Report No. 122, 54 pp, Acadia University, Wolfville, NS, Canada.

ACADIA ESTUARINE CENTRE FOR RESEARCH

Use of Fish Tracking Data to Model Striped Bass Turbine Encounter Probability in Minas Passage

Brian G. Sanderson and Anna M. Redden

29 September, 2016

Contents

Abstract

This project utilized fish tracking datasets and Vemco detection-range tests to calculate fish-turbine encounter probabilities for striped bass. Detection-range tests enables the probability of detecting a transmitted signal ρ to be empirically determined as a function of range, transmitter source level, and current speed. Detections of

tagged striped bass by receivers at the FORCE test site can be considered as an indication of how likely tagged striped bass are to be found in the vicinity where turbines are expected to be installed. The probability of detection ρ enables calculation of the effective area surounding a receiver that a transmission from a tagged fish is expected to be detected. Having calculated effective area and having measured detections of tagged striped bass, it is then possible to calculate abundance of tagged striped bass and thus the number that might encounter a hypothetical tidal turbine as they are swept along by the current over some time interval. Roughly speaking, detections by receivers are a proxy for encounters with turbines.

Tagged striped bass were determined to be of local Bay of Fundy origin, based on genetic analysis of 294 fin clip samples. The probability that a tagged striped bass encounters a turbine is, therefore, representative of encounters by the local population. The local population of striped bass has been estimated to be 15000. This number enables encounters by tagged striped bass to be converted into encounters by striped bass of the local population.

Presently we define encounter as the number of striped bass swept past a 16 m wide line at a position occupied by a hypothetical turbine that spans from top to bottom of the water column. This represents an overestimate that could be refined if the depth distributions of fish and turbine are specified. Different detection-range experiments give somewhat different values for probability of detection ρ and the number of encounters is inversely related to ρ. For example, during the month of July 2011 it was estimated that there would be 86 encounters at the FORCE site based on a detection-range test at the FORCE site but 233 encounters based on a detection-range test at the MPS receiver line.

Present estimates of monthly number of encounter do not represent the number of striped bass that would be harmed by a turbine. Many fish might pass either above or below the turbine. Some fish might avoid the turbine by swimming around it. Others might pass through the area swept by the turbine but still evade the blades. There is much uncertainty in the numbers calculated which can only be resolved by making further detection-range measurements.

1 Introduction

The use of Vemco acoustic telemetry technology has provided important advances in understanding temporal and spatial distribution of several fish species of conservation concern that move through the Minas Passage and Fundy Ocean Research for Energy (FORCE) Test Site for in-stream tidal turbine devices (Stokesbury et al 2012; Broome 2014; Redden et al 2014; Keyser 2015). One of the fish species examined, striped bass (*Morone saxatilis*), was detected moving within and through the Minas Passage during most of the year, including during winter when the extent of diel vertical migration was observed to decrease as temperatures dropped below 6°C (Keyser et al 2016). Should striped bass experience a lowered metabolic rate while in the Minas Passage during winter, then they may be at greater risk of direct interaction with tidal turbines.

An additional concern has been the origin of striped bass that move within and through Minas Passage. Conventional tagging studies have indicated that the composition of the striped bass aggregation in the upper Bay of Fundy is a mix of both US and Canadian origin striped bass (see Bradford et al 2015). To determine country of origin and relative use of the Minas Passage by US and local Canadian stocks, we included an analysis of the DNA from fin clip samples of 294 striped bass captured in the Minas Basin system. The results (see Appendix A, report from the Marine Gene Probe Laboratory, Dalhousie University) showed that all 164 striped bass that were implanted with Vemco tags during 2010-2012 were of Bay of Fundy origin, specifically the Stewiacke-Shubenacadie River system. Of the 294 striped bass examined, only one (58 cm fork length; captured at Grand Pre in summer of 2008) was considered to be a migrant from a US population.

Given the near year-round presence of Bay of Fundy striped bass in the Minas Passage, and their COSEWIC endangered status, the present work was undertaken to calculate the frequency with which striped bass would encounter a turbine located at the FORCE Test Site. The frequency with which tagged striped bass are detected by a Vemco receiver in the FORCE receiver array can be considered to be a qualitative indication of the rate at which fish encounter a turbine. In order to quantify fish-turbine encounter rate we must first know the range (distance) at which the tagged fish can be detected. Two detection-range experiments were undertaken. The first was at the FORCE Test Site from 10 October to 25 November 2009 and the second was at the MPS line from 10 August to 29 November 2010.

The detection-range experiments enable us to tabulate the probability ρ that a receiver will detect a transmitter at various ranges. This probability depends strongly upon tidal current. Given ρ, it is possible to determine the effective area from which a receiver will detect a tagged fish during a particular time of the tide. Such metrics can then be used to invert detection measurements to estimate the number of times that striped bass might encounter a turbine over some specified time interval. The fact that receivers were intensively deployed near the FORCE Test Site is particularly helpful for determining the potential for encounters at that site. For comparison, detections by receivers at other sites within Minas Passage will also be inverted to estimate fish-turbine encounters.

2 Detection Range Experiments

The two detection-range experiments are key to achieving our objective. The original purpose of the detection-range experiments was to calculate the efficiency with which arrays of receivers would detect fish passing by as they swim within the strong tidal currents in Minas Passage. This calculation will be reported elsewhere. Nevertheless, it is important for present purposes to carefully discuss some aspects of both the detection-range experiments and the acoustic technology. Additional information about the first detection-range experiment can be found in Broome (2014).

The VEMCO transmitters (acoustic tags) that were used for the detection-range measurements transmit a burst of 8 pulses. A pulse is obtained by amplitude modulation of a continuous-wave frequency of 69 kHz. Intervals between pulses are intended to identify the particular tag. This is called a period-encoding (Ehrenberg and Steig 2009). A successful detection requires that all 8 pulses are detected and that the intervals between pulses correspond to a tabulated tag identification number. Each pulse has duration of about 10 ms. Upon detecting a pulse the receiver blanks out any other received signals for 250 ms. Blanking is required in order to avoid 'detecting' echos of the received pulse that have been caused by reflections off the ocean floor or sea-surface (Pincock 2008). Thus from the beginning of one pulse to the beginning of the next pulse is typically > 300 ms and so the time taken to transmit a burst is 2.4 to 4 seconds.

2.1 Experiment 1, FORCE Test Site

The first detection-range experiment was undertaken within the FORCE Test Site from 10 October to 25 November 2009 (Figure 1). A line of 7 moorings was deployed along the major axis of the tidal flow and the centroid of the mooring locations was latitude 45.364065 N and -64.428298 W. Each mooring had an acoustic tag (transmitter) attached 1 m above a VEMCO receiver (Figure 2). Four types of tag were used (V16, V13, V9, V7) which have source levels $L_0 = (156, 153, 147, 136)$ dB respectively. Source level is with reference to a $\Phi_{\text{ref}} = 1$ μPa signal at a distance of $r_{\text{ref}} = 1$ m from the tag. Tags were set to have a delay of 480 s between bursts and the timing of bursts was offset by 120 s from one transmitter to the next in order to minimize signal interference. Broome (2014) reports that of the few signals that were rejected due to an invalid checksum, most were from a transmitter that was on the same mooring as the receiver.

2.2 Experiment 2, MPS line

The second detection-range experiment was undertaken from 10 August to 29 November 2010 by deploying transmitters at locations along the MPS line of receivers (Figure 1). This time the transmitters were on separate moorings from the receivers. Each transmitter was fitted and epoxied within a teflon[1] housing which was bolted through an 8 inch yellow trawl float (Figure 2) and attached to a 2 m riser that was, in turn, connected to a 45 kg mooring weight. Receivers were fitted within a 2-float SUB that was tethered to a heavy weight by a 2 m chain (Figure 2). This was the same configuration used for mooring receivers for fish detection.

Three V9 transmitters (1088185, 1088196, 1088197) were deployed between MPS-4 and MPS-5. The V9 tags were set to cycle through high/low power transmissions of 143/150 (dB re 1μPa at 1 m). Clock drift confounded separation of low and high power signals from transmitter 1088197 so an averaged power was assumed for all detections of that transmitter.

A V16 transmitter (1088202) was set to cycle through signals with powers of 153 and 160 dB. Unfortunately, the cycling sequence for the V16 was poorly chosen so that clock drift made it impossible to determine whether a received signal was from a high-power transmission or a low power transmission. Thus,

[1]The speed of sound in teflon, 1400 m/s, being similar to that in water.

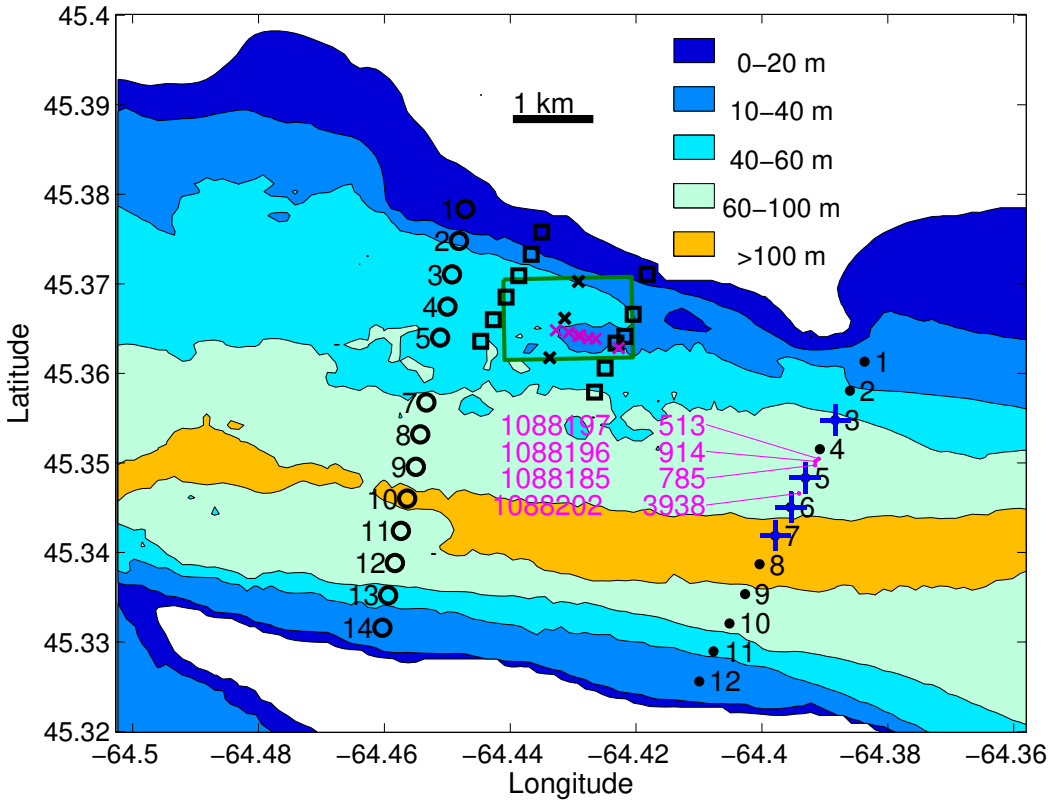

Figure 1: Bathymetry and receiver locations in Minas Passage. The FORCE Test Site which is marked by a dark green box. The 2009 range-testing moorings are marked by a line of 7 magenta crosses within the FORCE Test Site. The MPS receiver line is indicated by solid black dots numbered from 1 to 12 across the eastern end of the passage. The 2010 range-testing was done by mooring 4 transmitters (magenta lines point to each mooring) within the MPS line. The 2011 AUL-T line of tag receivers is marked with black crosses within the FORCE Test Site. The 2011 AUL line of receivers is marked with black circles, numbered 1 to 14 (receiver 6 was lost). The 2011/2012 MPS line of tag receivers is marked with black dots labelled 1 to 12. The two 2012 AUL lines of receivers are marked with black boxes at each end of the FORCE Test Site.

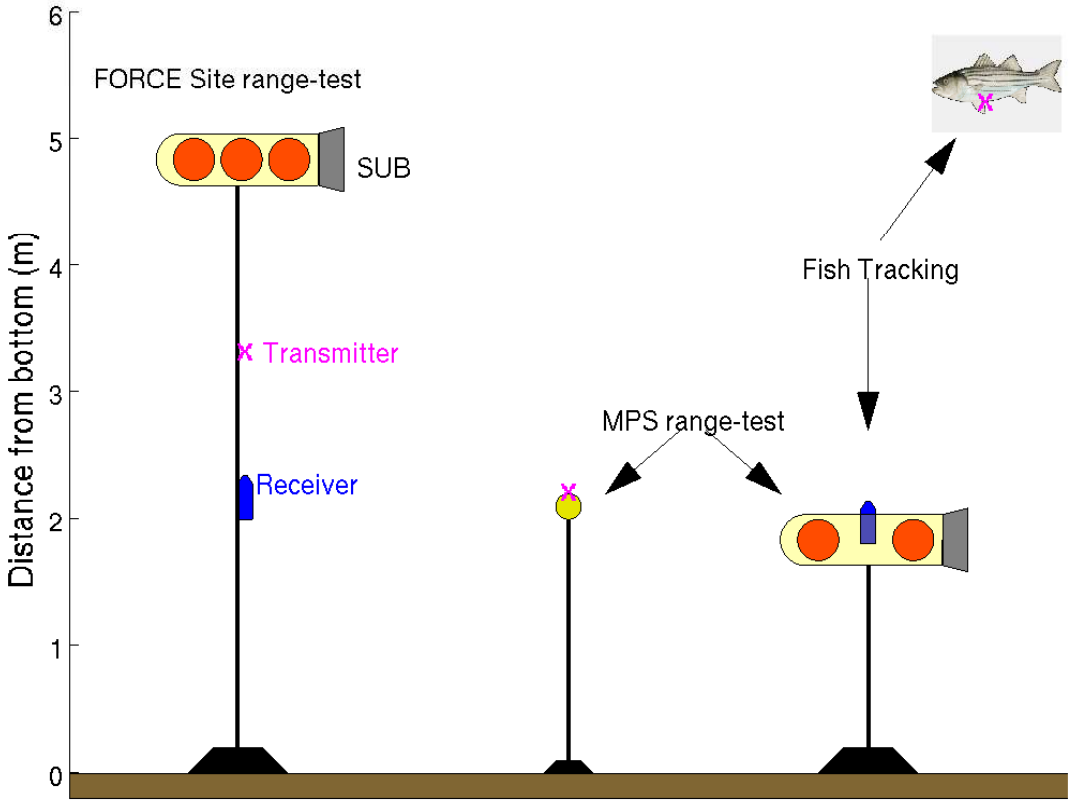

Figure 2: Schematic of the three types of mooring used for this project. Range-detection at the FORCE Test Site used the mooring design on the left, consisting of a SUB buoy that supports a transmitter 1 m above a VEMCO VR2w acoustic receiver. In this case, the streamlined housing of the SUB buoy encloses three 13" diameter VINY trawl floats for a total buoyancy of 60 kg. Range detection at the MPS line used a transmitter fastened to a 8" diameter buoy teathered 2 m above the bottom. The receiver was fastened through a SUB buoy, 2 m above the bottom, for both the MPS detection-range experiment and for fish tracking. In this later case the SUB buoy only enclosed two 13" diameter floats. Broome (2014) describes the mooring in detail.

for the purposes of the present analysis, all of the V16 transmissions were regarded as having power $(153 + 160)/2 = 156.5$ dB.

Unfortunately, receiver MPS-4 failed. Nevertheless, signals were received at sites 3, 5, 6 and 7 on the MPS line (blue plus signs in Figure 1) as documented in Table 1.

2.3 Experimental uncertainties

Given the strong currents in Minas Passage, there is always some degree of uncertainty in the location at which a mooring is deployed. Ranges from transmitter to receiver are, therefore, subject to a degree of uncertainty which we cannot specify but of which we must be cognizant.

Both receivers and transmitters are deployed close to the bottom, particularly for the second detection-range experiment. There is, therefore, the prospect that uneven bathymetry might interfer with line-of-sight paths between some transmitter-receiver pairs. Again, this is deemed more likely to be a problem for the second detection-range experiment than for the first.

Signal detection is expected to depend upon local levels of acoustic noise. Many things can cause acoustic noise. In the present experiment we expect that tidal currents, characteristics of the local bottom substrate, wind, waves, and rainfall might be implicated. The effects of these things are variable from time to time and/or also variable from place to place within Minas Passage. This introduces a degree of uncertainty comparing one experiment with the other and also causes uncertainty in the application of detection-range experiments to the interpretation of detections of tagged fish.

Receivers measure pressure fluctuations regardless of whether they are a sound wave or not. Strumming of mooring lines, advection of small particulates and turbulence can cause high-frequency pressure fluctuations (pseudo-sound) that do not propagate as sound but which a single receiver cannot differentiate from sound signals. Hydrophone measurements within the FORCE Test Site (Figure 1) confirmed that the combination of background sound and pseudo-sound were strongly related to tidal current speed (Figure 3). At the frequency used by the VEMCO tags (69 kHz), the spectral amplitude varies by at least 20 dB over the tidal cycle. We expect that reception of signals from tagged fish will depend very much upon the local current because background noise is much higher when currents are fast. Local bathymetric features and mooring design may also be relevant to contamination by pseudo-sound.

	TR	1088202	1088185	1088196	1088197
	Model	V16	V9	V9	V9
MPS	Low/High	160/153	150/143	150/143	150/143
1		0	0	0	0
2		0	0	0	0
3		0	14 (615)	349 (570)	178 (524)
	# Expected		3771/2516	3771/2514	6287
4		—	—	—	—
5		1680 (207)	713 (200)	552 (242)	335 (291)
	# Expected	9110	3984/2658	3984/2658	6642
6		1596 (200)	58 (603)	13 (646)	0
	# Expected	9110	3984/2658	3984/2658	
7		662 (601)	0	0	0
	# Expected	9110			
8		0	0	0	0
9		0	0	0	0
10		0	0	0	0
11		0	0	0	0
12		0	0	0	0

Table 1: Number of times each sentinel transmitter was detected at each receiver on the MPS line. The distance between transmitter and receiver is indicated within brackets. The receiver at MPS-4 failed. The expected number of low/high-power signals (# Expected) are also shown. For transmitters 1088202 and 1088197, it was not possible to reliably separate low-power signals from high-power signals so we show the total number expected. The receiver at MPS-3 was recovered early so the expected number of signals was less at that location.

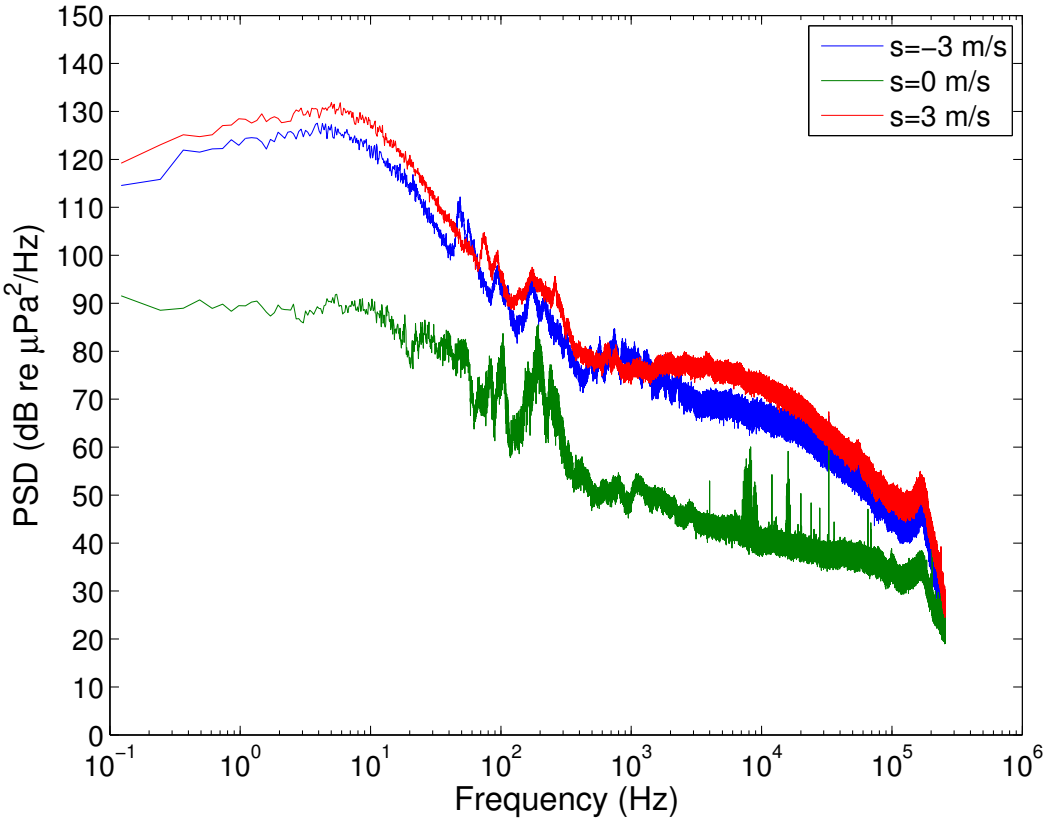

Figure 3: Spectra from an icListenHF that was attached to the Lander Platform on the volcanic platform at the FORCE Test Site. Spectra depend strongly upon vertically-averaged signed current speed s (positive for the flood tide, negative for the ebb tide).

The mooring configuration for fish tracking (Figure 2) *might* result in instrument tilt causing probability of detection ρ to be different for tagged fish that are upstream of the receiver than for tagged fish that are downstream. Neither of the range detection experiments are well designed to measure this effect and correct for it. In the case of the FORCE range detection measurements, tags were upstream and downstream but the flotation configuration with respect to the receiver is quite different from that used for fish tracking. The MPS range detection measurements had transmission paths that were aligned cross-stream.

Finally, there is always instrument uncertainty. Receivers cannot be expected to all perform equally. To test this, 6 pairs of VEMCO VR2w receivers were deployed in detection-range test at Kingsport from 17-19 August 2016. One receiver malfunctioned, otherwise the difference between receivers had a standard deviation that was about 5% of the average number of detections. The Kingsport measurements attached receivers to rebar driven into the sand/mud. When deployed in Minas Channel, attached to lines and buoys, transmitters may be subject to eratic motion which may cause additional variations in performance. Both transmitters and receivers are designed to be omnidirectional but cannot be expected to be perfectly omnidirectional, especially when they are configured with other objects on a wavering mooring.

3 Probability of Detection

The detection-range experiments measure when a transmitted signal is received and when it was expected but not received (Table 1 and Broome 2014). Signals are transmitted at various specified powers over ranges that can be calculated from the latitudes, longitudes and depths of the receivers and transmitters. A VEMCO Positioning System was deployed during the experiment at the FORCE Test Site but its performance was compromised by the extreme currents (Broome 2014).

Whether or not a signal is detected depends, in part, upon signal strength at the position of the receiver. Signal strength at the receiver, in turn, depends upon range and the power of the transmitter. Thus it makes sense to analyse the probabilities of detection in terms of the strength of the signal received.

Assume that both the transmitters and receivers are omnidirectional. De-

note the signal amplitude (pressure fluctuations) of the 69 kHz acoustic wave by the symbol Φ. Thus, the energy (proportional to Φ^2) in the transmitted signal spreads out over an area that increases as the square of range r^2. As the signal propagates, it is also attenuated due to sound absorption by seawater. Ignoring reflected signals, we can write

$$\Phi^2(r) = C\frac{\exp(-ar)}{r^2} \tag{1}$$

where C is a constant which need not be determined for present purposes and a is a coefficient of attenuation due to the absorption of sound energy by seawater. Although (1) is widely accepted physics, we have used an icListenHF to detect tags at various ranges and confirmed that it does, indeed, apply in an averaged sense — although, there is variability from one transmission burst to the next and, within each burst, pulse amplitude varies in apparently stochastic ways from one pulse to another (Sanderson personal observations made in Minas Basin). Potentially confounding circumstances include configurations when both transmitter and receiver are close to the bottom so the direct ray cannot be separated from a reflected ray or the rays may be blocked by variable bathymetry.

Using empirical formulae (Ainslie & McColm 1998, and Francois & Garrison 1982) we estimate that seawater absorption attenuates the energy of a 69kHz acoustic wave by about 19-22 dB/km. Attenuation varies depending upon depth, salinity, and temperature. In Minas Passage, variation of temperature is likely to cause the greatest changes in attenuation, with slightly more attenuation at higher water temperature. In the following work we will assume absorption causes 21 dB/km attenuation which corresponds to $a = 0.0048$ m^{-1} or an e-folding distance $1/a = 206$ m for Φ^2. (The e-folding distance for signal amplitude Φ is $1/(a/2) = 412$ m.)

At a reference range r_{ref} the signal is measured to be Φ_0 and (1) gives

$$\Phi_0^2 = C\frac{\exp(-ar_{\text{ref}})}{r_{\text{ref}}^2} \tag{2}$$

Decibels express Φ on a logarithmic scale relative to Φ_{ref} at r_{ref}

$$L(r) = 10\log_{10}\left(\frac{\Phi^2(r)}{\Phi_{\text{ref}}^2}\right) \tag{3}$$

Dividing (1) by (2)

$$\frac{\Phi^2}{\Phi_0^2} = \frac{\Phi^2/\Phi_{\text{ref}}^2}{\Phi_0^2/\Phi_{\text{ref}}^2} = \frac{\exp(-a(r-r_{\text{ref}}))}{(r/r_{\text{ref}})^2} \tag{4}$$

and applying the $10\log_{10}$ transform to both sides of the resulting equation gives

$$L(r) = L_0 - 0.021(r - r_{\text{ref}}) - 20\log_{10}(r/r_{\text{ref}}) \tag{5}$$

where the absorption term is written as $-0.021r$ and the range r is in units of metres. The convention for acoustics is to denote the sources level of an acoustic transmitter in decibels L_0 relative to $r_{\text{ref}} = 1$ m and $\Phi_{\text{ref}} = 1$ μPa. Equation (5) enables comparison between tags with different source levels at different ranges.

Equation (5) was used to collapse r and L_0 into a single variable L which is the strength of the signal (in decibels relative to 1 μPa at a reference range $r_{\text{ref}} = 1$ m) when it reaches the receiver location. Thus, the combinations of range and transmitter source levels result in a set of discrete values for L.

Detection probability also depends upon the current speed (Broome 2014). Currents were not measured during the detection-range experiments but Karsten et al., (2007) has modelled tidal currents that compare favourably with current measurements made in Minas Passage. Current velocity at the time and location of a tag detection (or the time of an expected detection) were otained by fitting tidal harmonics to vertically-averaged currents that were calculated by the model. Amplitude and phase of the tidal harmonics was then used to estimate current velocity at times and positions of interest.

In Minas Passage the dominant component of current is in the East-West sense with current in the positive x-direction corresponding to a flood tide and currents in the negative x-direction to an ebb tide. Signed current speed is defined as

$$s = \text{sgn}(u)\sqrt{u^2 + v^2} \tag{6}$$

where u is positive towards the East and v is positive towards the North. Thus, s is positive for the flood tide. Signed current speed, like u and v, represents a value that is averaged through the water column.

Each combination of transmitter and receiver corresponds to a unique value of L. For each L, the number of detections $N_{\text{detections}}$ and number of transmissions $N_{\text{transmissions}}$ were binned according to s. The bin-width for s was $\Delta s = 0.2$ m/s. Thus, for a given values of L and s we obtain the probability of detection is

$$\rho(L, s) = \frac{N_{\text{detections}}}{N_{\text{transmissions}}} \tag{7}$$

The first detection-range experiment gives $\rho(L, s)$ as shown in the top plot of Figure 4.

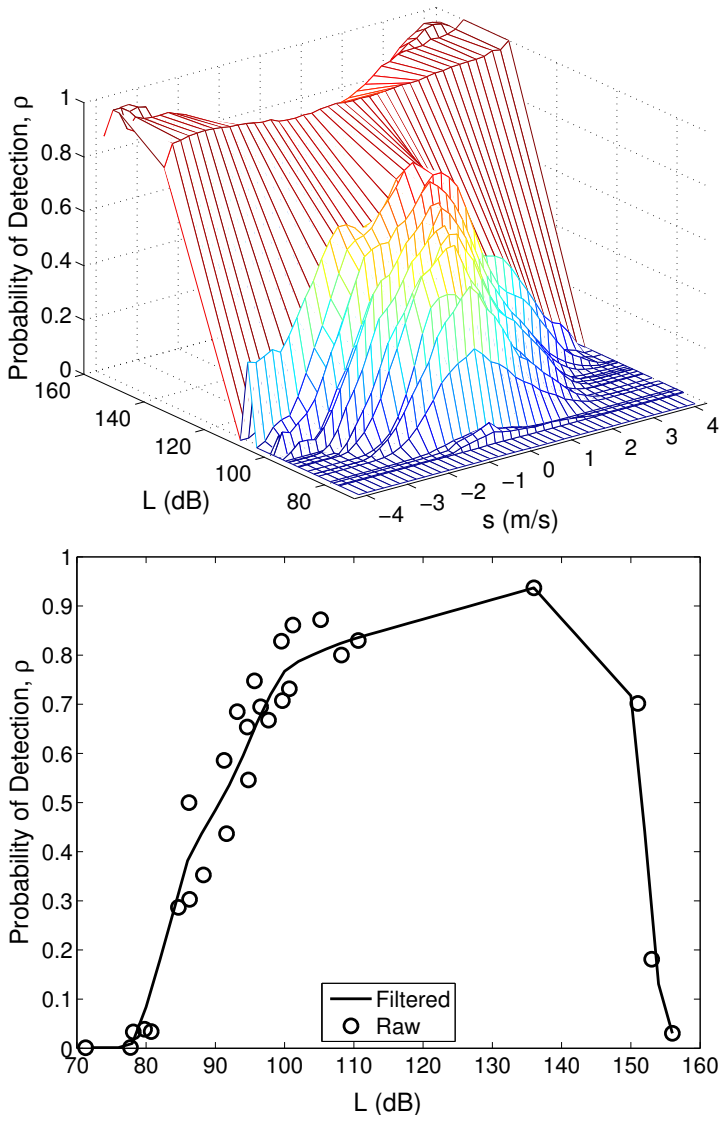

Figure 4: Results from the first range-test experiment (at the FORCE Test Site). Top: Measurements of probability of detection ρ plotted as a function of current speed and dB. Bottom: Probability of detection as a function of dB level when the signed current speed is -0.1 m/s. Circles show raw probabilities with the solid line obtained by applying a smoothing filter.

Figure 4 shows that probability of detection is a somewhat noisy function of L. This is most clearly shown by the lower plot in Figure 4. Such variability is expected because; the power of tags is not perfectly specified, different receivers may have different detection capabilities, bathymetry may be more favourable for some tranmission paths than others, and ambient sound (and/or pseudo-sound) may vary from one receiver location to the next. Given that such variability also exists for receivers and tags when they are used for fish tracking, it makes sense to estimate the underlying trend by smoothing out variability. This is done by applying a filter over the L dimension

$$\rho_i^{(\text{filt})} = \frac{(L_{i+1} - L_i)\rho_{i-1} + (L_{i+1} - L_{i-1})\rho_i + (L_i - L_{i-1})\rho_{i+1}}{2(L_{i+1} - L_{i-1})} \tag{8}$$

Equation (8) reduces to a 1-2-1 filter when probabilities are uniformly spaced with respect to dB. A 1-2-1 filter removes 2-Δ fluctuations but has little impact on larger scales (Purser and Leslie 1988). The filter is only be applied for $L < 110$. Multiple applications of the filter gives a smoothed estimate for the probability of detection which is represented by a black line in the lower plot of Figure 4.

Smoothing the top plot in Figure 4 along the L-axis for all current speeds gives an estimate for detection probability as shown by Figure 5. This plot represents a tabulated function for calculating probability of detection ρ as a function of L at the receiver and s at the detection-range site within the FORCE Test Site. Specific receivers or transmitters may perform better or worse than the tabulated function. The tabulated function for ρ captures the averaged performance. Generally, the probability of detection declines with range and also with increasing current speed.

The currents at the FORCE Test Site have an asymmetry, being stronger on the flood tide than on the ebb tide. For a given current speed, detection probability at the FORCE Test Site is higher on the ebb tide than on the flood tide. The reasons for this asymmetry are unclear. They could be caused by a systematic error in the modelled currents (eg underestimating the strength of the flood currents) or they might correspond to some physical phenomenon that is beyond the scope of our measurements to determine.

The first range-test experiment had a data gap for $112 < L < 136$ dB. In the absence of additional information, this gap was spanned by linear interpolation. Values of ρ where $L > 136$ dB are all obtained at a range $r \approx 1$ m that corresponds to the path between the transmitter and a receiver that

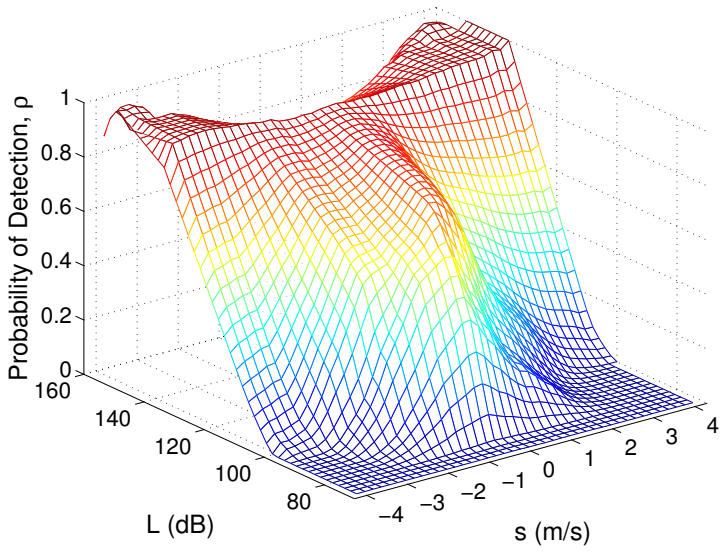

Figure 5: Probability of detection ρ after smoothing along the L-axis. These probabilities were found from the first range-test experiment which was conducted at the FORCE Test Site in October-November 2009.

is attached directly below on the same mooring (Figure 2). It is notable that at such short ranges the higher power transmitters have a lower probability of detection than lower power transmitters which is consistent with the close proximity detection interference observed by Kessel et al (2015). Also, at such very short ranges the detection probability improves at higher current speeds. This may have something to do with paths of signals reflected from the bottom/floats being changed when strong currents tilt the mooring.

The second detection-range experiment (at the MPS line) gave probability of detection as shown in the top plot of Figure 6. This second experiment did not include detections at close range. Again, there is variability with respect to L. Applying the smoothing operator (8) gives probability of detection as shown by the lighted surface in the lower plot of Figure 6. We overlay a semi-transparent mesh on this lower plot that represents the probability function obtained from the FORCE Test Site for a corresponding range of L. Clearly, the measurements at the FORCE Test Site indicate a significantly higher probability of detection, especially for larger current speeds. There are many reasons why this might be so. Moorings were differently configured and the

Statistic	MPS	FORCE < 110 dB	FORCE
std	0.05	0.06	0.07
max	0.18	0.16	0.35
min	-0.12	-0.18	-0.22

Table 2: Variations of smoothed detection probabilities from the measured values.

mooring arrays were differently aligned relative to current and bathymetry. The experiments were at different times, and the nature of the real currents (or the modelled currents) might be different at one location from the other. It seems unlikely that existing information[2] can be used to demonstrate why the two detection-range experiments gave different results. These differences should be framed within a perspective that includes other uncertainties.

The measured detection probabilities differ from their smoothed values as indicated in Table 2. Obviously the variations are not systematic in a way that can be exploited for calculating the detection efficiency of different tags that are implanted within moving fish by receivers at other locations. Smoothed detection probabilities are, therefore, more useful for analysing fish detections — albeit, with the proviso that for every instance there will be some unknowable variation of the probability of detection. Table 2 might be considered as loosely indicative of that uncertainty. (It would be misleading to pretend to be more precise.)

Ultimately, the reason for making detection-range measurements is to evaluate the efficiency with which transmissions from tagged fish are received. Tags that are implanted within the body cavity of a fish are anticipated to transmit with an effectiveness that is as good as (or better than) the tags used for the detection-range experiment at the FORCE Test Site — especially for fish that travel well clear of the bottom. The MPS detection-range experiment put the tag at a disadvantage by locating it closer to the bottom so that bathymetric variations become more likely to block the direct signal. Also, the MPS detection-range experiment attached tags to floats that were not streamlined and *may*, therefore, have been more unstable[3] in strong currents.

[2]Additional measurements have begun and are ongoing in order to investigate this matter. They will be briefly discussed in subsection 5.1.

[3]This issue may be resolved by a new detection-range experiment that is presently under way at the MPS line — using more streamlined flotation.

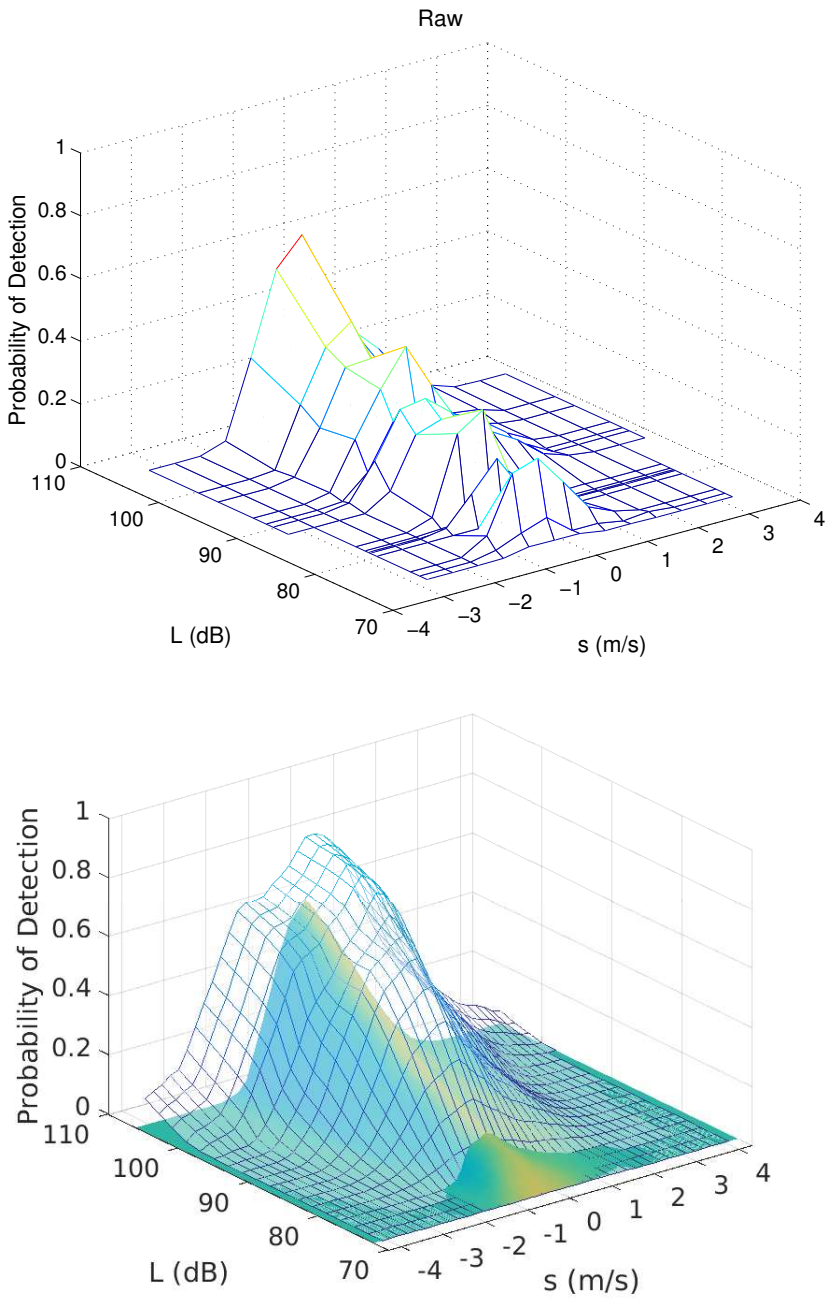

Figure 6: Probability of detection ρ as a function of L and signed current speed s. Top: Raw probabilities from the second detection-range experiment at the MPS-line. Bottom: Smoothed probabilities from the second-range detection experiment are shown with a lighted surface. The semi-transparent mesh shows smoothed probabilities from the detection-range experiment at the FORCE Test Site.

From the point of view of the receiver, the MPS detection-range experiment was the same as for the receivers deployed to track tagged fish — the receiver was housed within a modified SUB that had two VINY floats (Figure 2). The FORCE detection-range experiment had a more optimal configuration for the receiver (Figure 2) because: (1) It was clear of the flotation, (2) The flotation of the SUB was greater because three VINY floats could be used.

When L is large we only have values of ρ from the detection-range experiment at the FORCE Test Site. On the other hand, the MPS detection-range experiment extended to smaller values of L. The first thing to do is to see how the two data sets compare for that part of the L-domain in which they overlap.

Denote the MPS detection probability as ρ_{mps} and that from the FORCE site as ρ_{force}. Consider a scaling relationship

$$\rho_{\text{force}} = \alpha \rho_{\text{mps}}^{\beta} \tag{9}$$

which log-transforms to a form amenable for linear regression

$$\ln \rho_{\text{force}} = \beta \ln \rho_{\text{mps}} + \ln \alpha \tag{10}$$

Making the fit for those points where $\rho_{\text{mps}} > 0.05$ and $\rho_{\text{force}} > 0.05$ gives $\alpha = 1.4228$ (95% CI $1.2524 < \alpha < 1.6164$) and $\beta = 0.6757$ (95%CI $0.6085 < \beta < 0.7429$) where the R-square value is 0.6628 for the fit to the log-transformed quantities. These relationships will be used to map one set detection probability measurements onto the other.

The probability ρ from the MPS detection-range exeriment was scaled to match that from the detection-range experiment at the FORCE test site. Comparisons of probabilites then indicated that the MPS measurements could be used to slightly bolster FORCE detection probability when the range was large and the current speed low. Conversely, they indicated a reduction of FORCE detection probability at high current speeds and small range. The resulting function $\rho(L, s)$ is shown in Figure 7.

3.1 Detection of 10-pulse tags

Tags used for range testing transmitted a sequence (burst) of 8 CW-pulses. Thus, to successfully detect a tag, all 8 CW-pulses must be received and discriminated from background noise and also the intervals between pulses

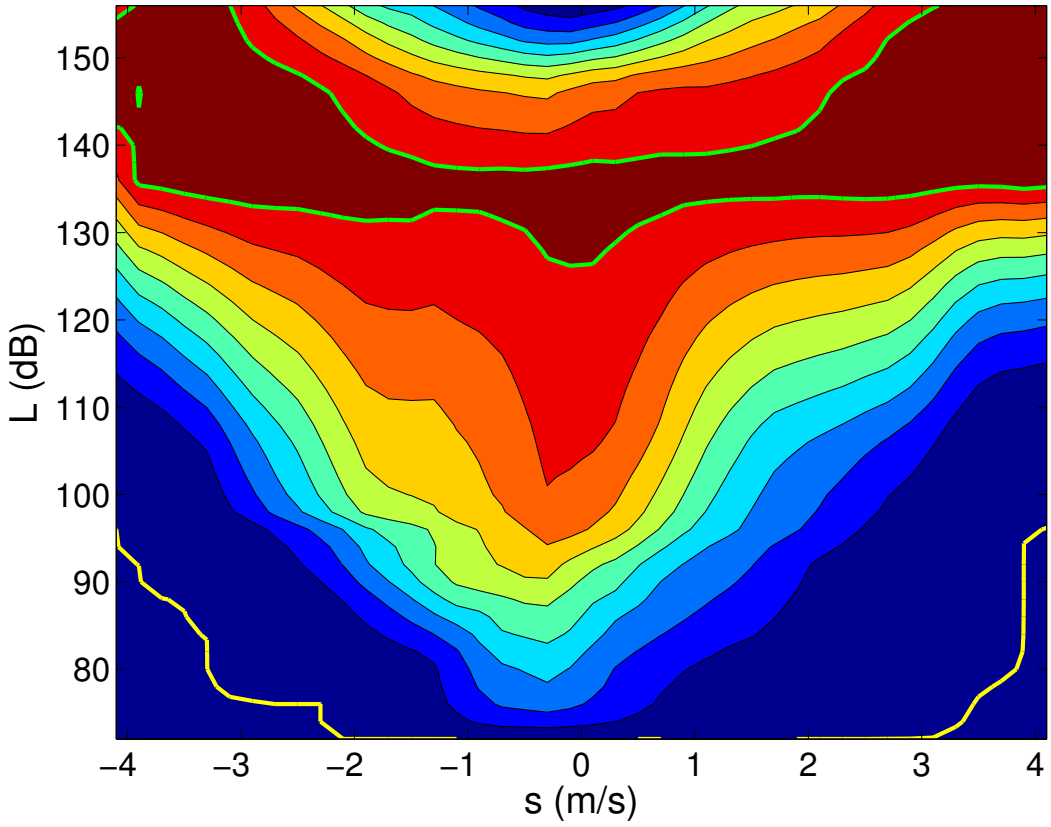

Figure 7: Modified FORCE probability of detection ρ at various dB with the distribution of current speed s. The contour interval is 0.1. The zero contour is plotted with a yellow line and the 0.9 contour in green.

must be consistent with a known transmitter. Subsequent to our range testing measurements, VEMCO introduced 10 CW-pulse tags in order to encode a greater number of tag identification numbers. The fish-tracking experiments were all done using 10-pulse tags.

Probabilities from the range test experiments have to be raised to a power of 10/8 in order to be applied to the 10-pulse tags. This somewhat reduces the probability of detection, although not in a linear way. If the probability of 8-pulse detection is ρ then the probability of 10-pulse detection is reduced to $\rho_{10} = \rho^{5/4}$. The maximum reduction in detection probability is obtained from

$$\frac{d(\rho - \rho_{10})}{d\rho} = 1 - \frac{5}{4}\rho^{1/4} = 0$$

The maximum decline in detection probability is $(4/5)^4 - (4/5)^5 \approx 0.182$ and it happens when $\rho = (4/5)^4 \approx 0.41$. Where the probability of detection is near 1 with the 8-pulse tags it will be little diferent from that for a 10-pulse tag. Similarly, where the probability was very low it will be little changed. All of the following calculations will transform ρ obtained from the detection-range experiments as appropriate for a 10-pulse tag.

It is also noteworthy that bursts of 10 pulses will take longer to transmit. Considering the blanking period after each pulse, the time taken to transmit a burst of 10 pulses is expected to be in the range 3 to 5 seconds.

4 Turbine Encounter

Ideally we would measure the trajectories of all fish approaching a turbine and observe any evasive maneuvers, strikes, and damage to the fish. Given the limitations of existing technologies and the difficulties imposed by physical conditions at the FORCE Test Site, it is hardly surprising that such measurements have yet to be achieved.

A few fish have been acoustically tagged and their signals sometimes detected by receivers moored at and near the FORCE Test Site in Minas Passage. How can we relate those observations to the probability that fish will encounter a turbine?

Begin by denoting the density of fish as F fish per unit area in the x-y plane. We have calculated the probability of detection $\rho(L, s)$ where L is related by (5) to the source level L_0 and distance r from the transmitter

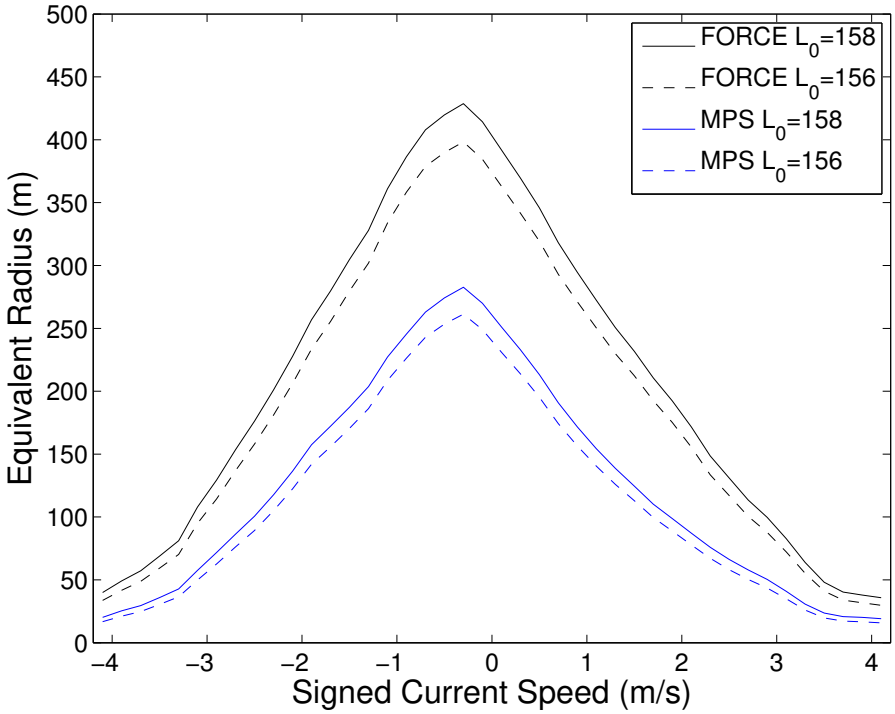

Figure 8: Equivalent radius $\sqrt{A_e/\pi}$ as a function of signed current speed. Values also depend upon the transmitter power L_0 and whether the probability of detection ρ is calculated according to the FORCE detection-range experiment or rescaled according to the MPS detection-range experiment.

to the turbine. Thus we can write the probability that a transmitted signal is detected by a receiver as $\rho(r, s|L_0)$. The effective area from which a transmission might be detected is

$$A_e = 2\pi \int_0^\infty \rho(r, s|L_0) r dr \tag{11}$$

At any given time t, we can determine the signed current speed $s(t)$ from tidal harmonics that have been fitted to modelled currents. Thus, we can calculate $A_e(x, y, t|L_0)$ for a particular receiver where the position and time dependence enters through the temporal variability of s. Figure 8 shows the equivalent radius $\sqrt{A_e/\pi}$ of the effective area of detection.

Let us denote $A_{e,i,k}(L_0)$ as the effective area about receiver i at time t_k.

Year Tagged Number Tagged	Model	Duration (d)	L_0 (dB re 1μPa 1 m)	τ (s)
2011				
40	V13P-1H	170	156	70
2012				
20	V13P-1H	170	156	70
8	V13P-1H	81	156	30
17	V16P-4H	774	158	70

Table 3: Tag information derived from metadata within Keyser (2015).

We have measured the number of detections of fish with tags that had a source level L_0 and were set to transmit at an average delay time τ. Keyser (2015) tabulates details regarding both receivers and tagged fish. In Table 3 we summarize tag information that has been derived from the metadata information contained in Keyser (2015).

The number of detections is expected to depend upon A_e and the density $\mathcal{F}$ of tagged fish. Obviously, only a small number of fish are tagged and they move through a large area. $\mathcal{F}$ is small. Keyser (2015) reports that fish are more likely to be in Minas Passage at some times of the year than others. In 2011 most of the receivers were only deployed for summer and fall and detections were more common in summer than fall. In 2012 the receivers were deployed for a more extended period and again there were more detections in summer than fall. Surprisingly, the 2012-2013 striped bass detections were most frequent in winter. It makes sense, therefore, to seek averaged values for the density of tagged fish on a month-by-month basis.

The number of detections that the receiver i makes during some time interval $[0, K\Delta t]$ is related to the averaged value of $\mathcal{F}$ by

$$N_i(T, L_0, \tau) = \mathcal{F}(T, L_0, \tau)\frac{1}{\tau}\sum_{k=1}^{K} A_{e,i,k}(L_0)\Delta t \tag{12}$$

where we have discretized the integration with respect to time $t_k = k\Delta t$. For fish tagged in 2011 the calculation is simple because tags all had the same value for transmitter power L_0 and delay τ. Thus measurements provide $N_i(T, L_0, \tau)$ and sampling effort $E_i(T, L_0, \tau)$

$$E_i = \frac{1}{\tau}\sum_{k=1}^{K} A_{e,i,k}(L_0)\Delta t$$

can be calculated from ρ and modelled currents. Thus we can calculate $\mathcal{F} = N_i/E_i$. In 2012 the fish were tagged with three (L_0, τ) tuples. The same method of calculation applies, only now it must be done separately for each tuple.

The density of tagged fish $\mathcal{F}_i(L_0, \tau)$ is related to the density of fish F_i by the ratio of the number of tagged fish $\mathcal{N}_{\text{tagged}}(L_0, \tau)$ to the population of fish $\mathcal{N}_{\text{population}}$. So, for the region and period of interest we obtain

$$F_i = \mathcal{F}_i(L_0, \tau) \frac{\mathcal{N}_{\text{population}}}{\mathcal{N}_{\text{tagged}}(L_0, \tau)} \tag{13}$$

Since all of the tagged striped bass were genetically found to have been spawned in the Shubenacadie-Stewiacke River system, we define $\mathcal{N}_{\text{population}}$ as the number of fish in that population. Douglas et al (2003) assessed that there were $\mathcal{N}_{\text{population}} > 15000$ striped bass of at least 3 years age. The total area of the Minas Channel, Minas Passage and Minas Basin is about 1600 km^2 so if the population were uniformly distributed over that area then there would be about 9.4 fish/km^2. There is no reason to believe that striped bass are uniformly distributed over that area — but it does, at least give us a simple scale which we can compare to results from acoustic tracking.

The expected number of fish that pass a turbine of some width W at location i is

$$N_p = F_i W |s| \delta t \tag{14}$$

in a time interval δt. N_p can be thought of as being the number of times fish encounter a turbine over some time span δt. We will refer to N_p as the number of fish-turbine encounters, (abbreviated to "encounter #") that happen over a time δt of one month. The rate at which fish encounter a turbine is $N_p/\delta t$ and is numerically the same as N_p if we talk in terms of the number of fish-turbine encounters per month. Fish that encounter a turbine in this way may pass harmlessly above, below, around or even through the turbine. Relating N_p to fish strikes[4], or fish mortality, is beyond the scope of what can be calculated from existing information.

Estimates of turbine-fish encounters are of particular interest for the FORCE Test Site. In 2011 the AUL-T line consisted of three VEMCO receivers that were deployed within the FORCE Test Site (black crosses in Figure 1). For each of the months from May to Nov 2011 we calculated the

[4]A framework for considering such matters will be discussed in subsection 5.2.

Month 2011	Tagged #	Detect-ions #	$\sum_i \sum_k A_{e,i,k}$ (km^2)	F (fish/km^2)	Encounter #
May	4.02	0	**31148** (11522)	**0** (0)	—
Jun	23.3	52	**29779** (11005)	**1.12** (3.04)	**87** (235)
Jul	40	85	**30146** (11126)	**1.06** (2.86)	**86** (233)
Aug	40	47	**29749** (10979)	**0.59** (1.61)	**49** (133)
Sep	40	3	**22621** (8333)	**0.050** (0.14)	**4** (11)
Oct	40	11	**15907** (5850)	**0.26** (0.71)	**22** (59)
Nov	40	2	**2398** (889)	**0.31** (0.84)	**25** (67)

Table 4: Estimated number of encounters of striped bass with a 16 m diameter tidal turbine $W = 16$ m at the FORCE Test Site in 2011. Obtained from detections made by the VEMCO receivers that were deployed at AUL-T1-3 stations during 2011. The FORCE scaling of ρ was used to calculate the numbers indicated by **bold type** whereas the MPS scaling of ρ was used to calculated bracketed numbers.

average number of tagged fish that were in the water for that month and compared that with the total number of detections by the three AUL-T receivers during each month and the effective area sampled by those receivers $\sum_k \sum_i A_{e,i,k}$. These quantities are given in columns 2, 3 and 4 of Table 4. The fifth column shows the calculated density of fish F and the sixth shows the number of encounters with a turbine that might be expected during each month. Numbers in bold are calculated assuming that ρ is scaled according to the detection-range experiment at the FORCE Test Site whereas the bracketed numbers are for ρ scaled according to the detection-range measurements at the MPS line.

Values of F in Table 4 are considerably smaller than the 9.4 fish/km^2 that was estimated on the assumption of a uniformly distributed population of 15000 striped bass. Nevertheless, the number of encounters with a single turbine is not insignificant, particularly in June and July. The MPS scaling of ρ indicates increased fish density (but still much less than 9.4 fish/km^2) and more turbine encounters because smaller values of ρ correspond to a smaller area being sampled by the receivers. Some care must be taken interpreting the results for May. Only a few fish were tagged in May (in Stewiacke River) > 70 km from Minas Passage.

In 2011, the relatively low values of F at the FORCE Test Site beg the question: Where are all the striped bass? In that year there were two lines of

Month 2011	Tagged #	Detect-ions #	$\sum_i \sum_k A_{e,i,k}$ (km^2)	F (fish/km^2)	Encounter #
May	4.02	0	**115685** (42826)	**0** (0)	—
Jun	23.3	322	**110228** (40758)	**1.88** (5.08)	**145** (393)
Jul	40	577	**111198** (41038)	**1.95** (5.27)	**159** (429)
Aug	40	229	**106422** (39268)	**0.81** (2.19)	**67** (181)
Sep	40	87	**93303** (34448)	**0.35** (0.95)	**28** (76)
Oct	40	26	**84628** (31150)	**0.12** (0.31)	**10** (26)
Nov	40	20	**70241** (25869)	**0.11** (0.29)	**8** (23)

Table 5: Number of encounters estimated from tag detections by VEMCO receivers along the AUL-line in 2011. A 16 m diameter tidal turbine $W = 16$ m is assumed. The FORCE scaling of ρ was used to calculate numbers in **bold type** and bracketed numbers were calculated using MPS scaling of ρ.

Month 2011	Tagged #	Detect-ions #	$\sum_k \sum_i A_{e,i,k}$ (km^2)	F (fish/km^2)	Encounters #
May	4.02	0	**98880** (36851)	**0** (0)	—
Jun	23.3	526	**94622** (35235)	**3.57** (9.59)	**276** (742)
Jul	40	688	**95483** (35478)	**2.70** (7.27)	**224** (592)
Aug	40	243	**93476** (34723)	**0.98** (2.62)	**81** (217)
Sep	40	9	**90369** (33610)	**0.04** (0.10)	**3** (8)
Oct	40	113	**92965** (34609)	**0.46** (1.22)	**38** (101)
Nov	40	143	**84594** (31597)	**0.63** (1.7)	**50** (134)

Table 6: Number of encounters estimated from tag detections by VEMCO receivers along the MPS-line in 2011. A 16 m diameter tidal turbine $W = 16$ m is assumed. The FORCE scaling of ρ was used to calculate numbers in **bold type** and bracketed numbers were calculated using MPS scaling of ρ.

receivers spanning Minas Passage: The AUL-line to the west and the MPS-line to the right (Figure 1). Table 5 shows fish density and encounters are, arguably, a little higher in the AUL-line than at the FORCE Test Site. To the east, the MPS-line has much higher values for fish density (Table 6). It seems reasonable to propose that the striped bass population may have been distributed more within Minas Basin when the 2011 measurements were made. Keyser (2015) found striped bass had higher residency at specific sites within the Lower Southern Bight of Minas Basin than at specific sites within Minas Passage. Quantitative comparison of residency measurements is confounded by the difficulty that the ρ that applies to Minas Passage might be quite different[5] from the ρ that applies to receivers deployed near the low tide level within Minas Basin. Nevertheless, the results of Keyser (2015) offer qualitative support for our proposition.

In 2012 striped bass were tagged and tracked for a longer period which extended from May 2012 to April 2013. The AUL receivers were positioned in two lines across the western and eastern sides of the FORCE Test Site (Figure 1). Fish densities and fish-turbine encounters at the FORCE Test Site were lower in June, July and August of 2012 (Table 7) than they had been for those months in 2011. There is significant year to year variability.

High fish densities and fish-turbine encounters were obtained during the colder months at the FORCE Test Site in 2012/2013 (Table 7). Even higher values were obtained at those times along the MPS line (Table 8).

5 Discussion

Whereas striped bass have been tracked during two summer/fall seasons, they have only been tracked for one winter. Given the difference observed from one summer/fall to the next, we can only caution that we don't know how fish densities and encounter rates might vary from one winter to the next.

Fish-turbine encounter N_p depends upon the number of fish $\mathcal{N}_{\text{population}}$ in the population. We set $\mathcal{N}_{\text{population}} = 15000$ as a rough estimate based on

[5]Indeed, a 17-19 August 2016 detection-range experiment made at Kingsport indicated that detection efficiency in Minas Basin was not degraded by strong currents (Sanderson unpublished work) whereas it is in Minas Passage. On the other hand, there was an indication that salinity variations associated with intermittent catchment discharge can sometimes degrade the detection efficiency near the shores of Minas Basin.

Month 2012	Tagged #	Detect-ions #	$\sum_k \sum_i A_{e,i,k}$ (km^2)	F (fish/km^2)	Encounters #
May	2.25	0	**160649** (60437)	**0** (0)	—
Jun	23.4	11	**155072** (58378)	**0.05** (0.12)	**4** (10)
Jul	40	349	**160622** (60509)	**0.82** (2.16)	**67** (178)
Aug	45	21	**160414** (60484)	**0.04** (0.12)	**4** (10)
Sep	42.1	21	**146612** (55290)	**0.05** (0.14)	**4** (11)
Oct	37	171	**151603** (57158)	**0.46** (1.21)	**37** (99)
Nov	37	190	**131508** (49292)	**0.59** (1.56)	**46** (123)
Dec	37	429	**120624** (44674)	**1.44** (3.89)	**117** (317)
2013					
Jan	19.7	678	**121204** (44887)	**4.27** (11.5)	**352** (948)
Feb	17	380	**103118** (38260)	**3.25** (8.79)	**239** (645)
Mar	17	509	**109233** (40441)	**4.11** (11.1)	**343** (927)
Apr	17	33	**97530** (36154)	**0.30** (0.81)	**24** (65)

Table 7: Calculated number of encounters of striped bass with a 16 m diameter turbine (W = 16 m) at the FORCE Test Site. Calculations were made using detections by VEMCO receivers at the 2012-2013 AUL stations All these stations are within the FORCE Test Site. FORCE scaling of ρ was used to calculate the numbers in **bold type**. Bracketed numbers were calculated using MPS scaling of ρ.

Month 2012	Tagged #	Detect-ions #	$\sum_k \sum_i A_{e,i,k}$ (km^2)	F (fish/km^2)	Encounters #
May	2.25	0	**175422** (66368)	**0** (0)	—
Jun	23.4	60	**169153** (64014)	**0.23** (0.60)	**18** (48)
Jul	40	228	**174240** (65926)	**0.49** (1.30)	**41** (107)
Aug	45	65	**118740** (44868)	**0.18** (0.48)	**15** (40)
Sep	42.1	115	**114456** (43243)	**0.36** (0.95)	**28** (75)
Oct	37	105	**118844** (44930)	**0.36** (0.95)	**29** (77)
Nov	37	565	**115654** (43763)	**2.0** (5.23)	**155** (411)
Dec	37	1416	**119248** (45146)	**4.8** (12.7)	**393** (1038)
2013					
Jan	19.7	1214	**118562** (44888)	**7.8** (20.6)	**645** (1698)
Feb	17	375	**107625** (40743)	**3.1** (8.12)	**226** (598)
Mar	17	1192	**116918** (44155)	**9** (23.8)	**752** (1988)
Apr	17	12	**34585** (12980)	**0.31** (0.82)	**25** (66)

Table 8: Number of encounters estimated from tag detections by VEMCO receivers along the 2012-2013 MPS line of stations at the eastern end of Minas Passage. A 16 m diameter tidal turbine $W = 16$ m is assumed. FORCE scaling of ρ was used to calculate the numbers in **bold type**. Bracketed numbers were calculated using MPS scaling of ρ.

Douglas et al (2003). Population dynamicists might be more interested in the fish-turbine encounters per fish in the population, that is $N_p/\mathcal{N}_{\text{population}}$. The highest number of encounters in a month at the FORCE Test Site was 352 in January 2013. This translates to a probability of $352/15000 \approx 0.02$ that a striped bass would encounter a turbine at some time during that month. This probability is more robustly known than the number of fish-turbine encounters N_p because it cancels uncertainty in our knowledge of the population of striped bass (which appears in F_i). Nevertheless, uncertainty remains high because only a tiny fraction of the population has been acoustically tagged and tracking measurements have only been made for a small fraction of the life span that a striped bass might achieve.

Winter water temperatures approach the limits that striped bass are believed to be capable of enduring. Under aquacultured conditions, striped bass stop feeding and become inactive before temperature drops to winter time values. It is quite possible — but *not demonstrated* — that the striped bass that we detected during winter may have limited ability to avoid turbines when they encounter them.

The 2012 tracking measurements dispell conventional wisdom that striped bass either migrate outwards from the inner Bay of Fundy for the winter or overwinter under ice in the Shubenacadie Grand Lake. It appears that many striped bass overwinter in Minas Passage and adjacent waters. It has not been determined what fraction of the population spends winter in the Minas Basin-Passage-Channel or how that fraction might vary from one winter to the next. This fraction is another important number to know[6] if we are to more accurately assess the rate with which striped bass encounter turbines during the winter.

Although we have calculated quantities averaged over each month, variability can be assumed over all time scales and from place to place. It may well be that long periods with few encounters are sometimes punctuated by events with many encounters. We caution that the present estimates for fish-turbine encounter number are just what was measured at a few places for a few time intervals. We should be wary about extrapolating the present results to other times and other places.

Presently we report the number of encounters based upon an estimated 15000 striped bass of at least 3 years age. This estimate was made more than a decade ago (Douglas et al, 2003) and assumed that the entire popula-

[6]It is also important to know the population abundance and size structure.

tion overwintered in the freshwaters of the Shubenacadie-Stewiacke system. The population might well have changed since then. Recently, Redden et al (2014) found that some striped bass overwinter in Minas Passage which introduces some ambiguity about how the 15000 number should be interpreted. It would be straighforward to rescale the present results should new measurements of the striped bass population become available. For example, the number of encounters can be converted to a probability of encounter for one striped bass (encounters/15000) which can then be multiplied by the newly measured population to obtain the rescaled value for the expected number of encounters. One must qualify such calculations, however, because behaviour might change as population changes.

5.1 Looking forward

The following is looking forward, far beyond the scope of the present project, but with a view of what will be ultimately required in order to evaluate fish-turbine encounters and interactions.

The scope of the present study was restricted to striped bass. Atlantic sturgeon have also been acoustically tagged and detected in Minas Passage and Minas Basin. The presently developed methods are expected to be applicable to Atlantic sturgeon. Furthermore, the present methods enable both estimates of local abundance F_i and rates of encounter to be estimated at other locations where VEMCO VR2w receivers have been deployed. It is very relevant to determine F_i at locations within Minas Basin as well as at the FORCE Test Site and other locations in Minas Passage because this would give an indication of the extent to which populations of these species are collocated with turbine sites.

A good understanding of appropriately made detection-range measurements is critical to the task of inverting detections of both striped bass and Atlantic sturgeon so as to obtain their local abundance F_i and knowledge of fish-turbine encounters. Presently, we have done what we can with the information at hand. Further measurements that are required to fully exploit the existing fish detection measurements are as follows:

- Detection-range measurements at Kingsport and drifter-based detection-range measurements in Minas Basin. These serve to obtain estimates of F_i for striped bass and sturgeon at VR2w sites within Minas Basin.

- A second detection-range experiment on the MPS line[7], using a better mooring design (since that was considered to be a reason why previously obtained detection probability was low at that site). Drifter-based detection-range measurements in Minas Passage. This work is presently ongoing. Results will better tie down our estimates of fish-turbine encounters and F. In particular, it is hoped that values of F will be better determined at the MPS line for comparison with the FORCE Test Site and Minas Basin.

- Drifter-hydrophone measurements of ambient sound in Minas Basin and at the different sites in Minas Passage. These measurements have multiple utility. In the present context, they provide a basis for knowing the extent of psuedo-sound vs ambient sound. Such knowledge is important for determining the extent to which improved mooring design[8] might lead to improved tracking of acoustically tagged fish in high flow waters.

An OpenHydro turbine to be installed at FORCE by Cape Sharp Tidal in 2016 will include an acoustic imaging system, oriented towards Minas Basin, which will image fish approaching the turbine during ebb tide. The presently calculated rate of fish-turbine encounter does not directly transcribe to an estimate of the rate at which striped bass might be expected to enter within the field that is scanned by the acoustic imaging system but it is indicative. Given the field of view for the acoustic imaging system, the presently discussed methods can be adapted in order to estimate how many striped bass the imaging system might be expected to detect over some period of time. A sufficiently substantial difference between the expected number of imaging detections and the actual number of detections might be interpreted as a behavioural response (attraction or avoidance) of striped bass to the turbine installation.

5.2 Beyond encounters

Our measure of encounter includes all striped bass that pass at any depth across a line that is the width of the turbine. It follows that many fish will

[7]Undertaken thanks to the Ocean Tracking Network

[8]Substantial improvements are possible, although not without some development effort. These measurements would indicate whether or not the effort would be cost-effective.

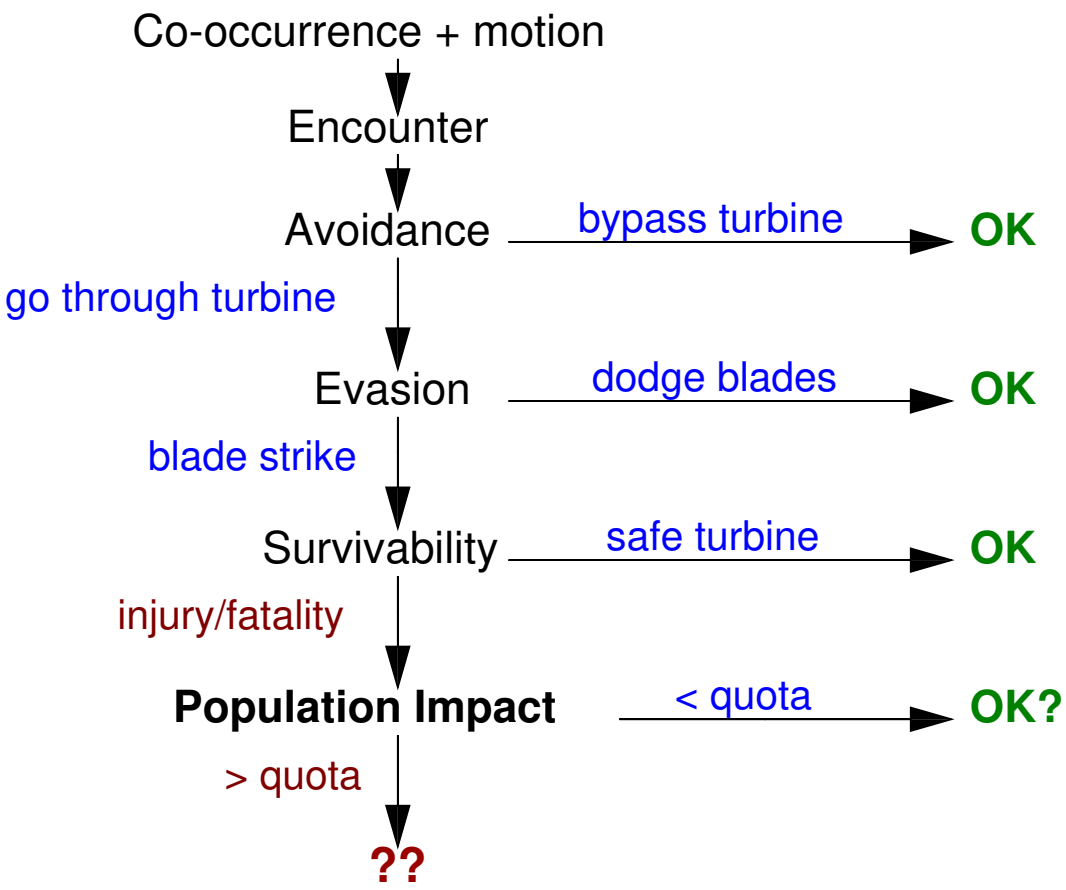

Figure 9: Schematic of the range of fish-turbine interactions and possible outcomes and uncertainties from such interactions. Schematic is loosely based upon Hammar et al (2015) with additional considerations regarding population dynamics and fishery management.

be at levels that are sufficiently high or low so that they are harmlessly swept past the turbine without taking any evasive action. Additionally, the same geometric constraints that give us Betz limit also ensure that some of the upstream flow is pushed aside, around the turbine, harmlessly carrying fish with it.

It would be entirely inappropriate to jump from our admittedly crude estimates of F_i and N_p and draw conclusions about the harm that turbines do or don't do to fish. Figure 9 is one way to illustrate this point. While F_i is relevant to the co-occurrence of fish and turbines and contributes to estimates of fish-turbine encounters N_p, it is only the first part of any logical analysis that will be required to assess whatever danger (perhaps none) that a specific turbine poses to a specific species of fish at some specific tidal site. Fish might detect the turbine from sufficiently far upstream and be motivated to avoid it (*Avoidance* in the diagram). Or, they may pass through the turbine but detect and dodge the blades (*Evasion* in the diagram). Even without avoidance or evasion, a blade strike might be survivable (*Survivability* in the diagram), or not. Finally, to be consistent with the principes of fisheries management and resource management in general, we must consider the impact of turbine installations upon fish populations. Just as fishers are assigned a quota that is deemed to be "sustainable", so might turbine installations.

The extent to which striped bass can detect and avoid a turbine is largely unknown. We anticipate that avoidance and evasion will vary from one species to another and will also from site to site and will be different from time to time and from one turbine design to another. Survivability of a blade strike is known to depend upon blade speed and the shape and thickness of the leading edge relative to the length of the fish. Some species of fish are more robust than others.

There may not always be a need to know avoidance, evasion or survivability. In some circumstances it is possible that fish-turbine encounter rates and population dynamics are sufficient to determine whether or not turbines will cause a population change that is within an acceptable range.

References

[1] Ainslie M.A., McColm J.G., 1998. A simplified formula for viscous and chemical absorption in sea water, Journal of the Acoustical Society of

America, 103(3), 1671-1672.

[2] Bradford, R.G., Halfyard, E.A., Hayman, T., and LeBlanc, P. 2015. Overview of 2013 Bay of Fundy Striped Bass Biology and General Status. DFO Can. Sci. Advis. Sec. Res. Doc. 2015/24. iv38.

[3] Broome, J.E. 2014. Population Characteristics of Striped Bass (*Morone saxatilis*, Walbaum 1792) in Minas Basin and Patterns of Acoustically Detected Movements within Minas Passage. M.Sc. Thesis, Acadia University.

[4] Douglas, S.G., Bradford, R.G., and Chaput, G. 2003. Assessment of striped bass (*Morone saxatilis*) in the Maritime Provinces in the context of species at risk. DFO Can. Sci. Advis. Sec. Res. Doc. 2003/008. 1-49.

[5] Ehrenberg, J.E. and T.W. Steig. 2009. A study of the relationship between tag-signal characteristics and achievable performances in acoustic fish-tag studies. International Council for the Exploration of the Sea. ICES Journal of Marine Science, 66(6): 1278-1283.

[6] Francois R.E., Garrison G.R. 1982. Sound absorption based on ocean measurements: Part I: Pure water and magnesium sulfate contributions, Journal of the Acoustical Society of America, 72(3), 896-907.

[7] FORCE 2012. Fundy Ocean Research Center for Energy Annual Report 2011. www.fundyforce.ca/wp-content/uploads/2012/05/2011-FORCE-Annual-Report.pdf

[8] Hammar L., Eggertsen L., Andersson S., Ehnberg J., Arvidsson R., Gullstrom M. 2015. A Probabilistic Model for Hydrokinetic Turbine Collision Risks: Exploring Impacts on Fish. PLoS ONE 10(3): e0117756. doi:10.1371/journal.pone.0117756

[9] Karsten, R.H., McMillan, J.M., Lickley, M.J., Haynes, R.D. 2007. Assessment of tidal current energy in the Minas Passage,Bay of Fundy, J. Power and Energy, 222: 493-507. DOI: 10.1243/09576509JPE555

[10] Kessel, S.T., Hussey, N.E., Webber, D.M., Gruber, S.H., Young, J.M., Smale, M.J., and Fisk, A.T. 2015. Close proximity detection interference

with acoustic telemetry: the importance of considering tag power output in low ambient noise environments. Animal Biotelemetry 3:5. DOI 10.1186/s40317-015-0023-1

[11] Keyser, F.M., 2015. Patterns in the Movement and Distribution of Striped Bass (*Morone saxatilis*) in Minas Basin and Minas Passage. MSc Thesis, Acadia University. 155 pp.

[12] Keyser, F.M., J.E. Broome, R.G. Bradford, B. Sanderson, and A.M. Redden. 2016. Winter presence and temperature-related diel vertical migration of Striped Bass *Morone saxatilis* at and near a tidal energy turbine test site in Minas Passage, Bay of Fundy. Canadian Journal of Fisheries and Aquatic Sciences. Published on the web 02 June 2016, 10.1139/cjfas-2016-0002

[13] Pincock, D.G. 2008. Understanding the Performance of VEMCO 69 kHz Single Frequency Acoustic Telemetry. Document #:XDOC-004372 Version 05, February 19, 2008, AMIRIX Systems Inc, 77 Chain Lake Drive, Halifax, NS B3S 1E1.

[14] Pincock, D., D. Welch, S. McKinley, G. Jackson. 2010. Chapter 6. Acoustic Telemetry for Studying Migration Movements of Small Fish in Rivers and the Ocean-Current Capabilities and Future Possibilities, *In* PNAMP Special Publication 2010-002: Tagging, Telemetry, and Marking Measures for Monitoring Fish Populations. *Eds* Wolf, K.S. and J.S. O'Neal.

[15] Purser, R.J., and L.M. Leslie 1988. A semi-implicit, semi-Lagrangian, finite-difference scheme using high-order spatial differencing on a nonstaggered grid. Monthly Weather Review, 116, 2069-2080.

[16] Redden, A.M., M.J.W. Stokesbury, J.E. Broome, F.M. Keyser, A.J.F. Gibson, E.A. Halfyard, M.F. McLean, R. Bradford, M.J. Dadswell, B. Sanderson and R. Karsten. (2014). Acoustic tracking of fish movements in the Minas Passage and FORCE Demonstration Area: Pre-turbine Baseline Studies (2011-2013). Final Report to the Offshore Energy Research Association of Nova Scotia and Fundy Ocean Research Centre for Energy. Acadia Centre for Estuarine Research Technical Report No. 118, Acadia University, Wolfville, NS. 153p

[17] Stokesbury, M.J.W., J.E. Broome, A.M. Redden, and M. McLean. 2012. Acoustic tracking of Striped Bass, Atlantic Sturgeon and American Eel in the Minas Passage. Phase 2 of 3 in the report on 3-D acoustic tracking of fish, sediment-laden ice, and large wood debris in the Minas Passage of the Bay of Fundy, submitted to the OERA. ACER Technical Report 108, 40 pp.

APPENDIX A

Genetic Analysis of Striped Bass Samples

Report on genetic analysis of striped bass, *Morone saxatalis* captured in the Bay of Fundy

Paul Bentzen
Ian Paterson

Marine Gene Probe Laboratory,
Dalhousie University,
Halifax Nova Scotia

March 22, 2016

Introduction

Striped bass (*Morone saxatilis*) are native to much of the east coast of North America, and undertake lengthy and complex migrations in both fresh and marine waters (COSEWIC 2012). A consequence is that striped bass sub-adults and adults encountered in either marine and freshwater habitats in Atlantic Canada can be of local origin, or they may be migrants from relatively distant U.S. populations. Historically, striped bass spawned in at least five rivers in Atlantic Canada: St. Lawrence, Miramichi, Shubenacadie (and Stewiacke), Saint John, and Annapolis (COSEWIC 2012. Of these spawning populations, the St. Lawrence and Annapolis populations are thought to have been extinct for many decades. The Saint John River population was also believed to have disappeared several decades ago, although genetic data suggest that a small remnant population may exist (Bentzen *et al*. 2009; Bradford *et al*. 2012).

Notwithstanding the possibility of a remnant Saint John River population, striped bass encountered in the Bay of Fundy or small rivers that drain into it are likely to be of either Shubenacadie/Stewiacke origin, or from U.S. populations. There is little evidence from genetic data that striped bass from the Miramichi population migrate to the Bay of Fundy (Bentzen *et al.* 2009, Bentzen unpublished data).

Here we report on genotypic data from 294 striped bass captured in the upper Bay of Fundy region. Using genetic from reference collections of striped bass from the Shubenacadie/Stewiacke, Miramichi and several U.S. populations, we carry out Bayesian clustering on the new striped bass samples in order to infer their most likely population(s) of origin.

Methods

Genomic DNA was isolated from 294 striped bass samples following the method of Elphinstone et al. (2003). Genetic data were collected for eight microsatellite loci using primers listed in Table 1. Microsatellite loci were amplified for genotyping in two stages. First, locus-specific primers were used to amplify all eight loci in a single multiplex polymerase chain reaction (PCR); then, a second index PCR was conducted to incorporate the 6-base sample specific index sequences and Illumina annealing sequences to enable DNA sequencing.

Multiplex PCRs were performed in a single 3.5µL reaction using the following conditions; 1.75µL Qiagen Type-it Microsatellite PCR 2x master mix (Qiagen, Toronto ON), 0.1µM each primer and 0.5µL of DNA. PCR cycling conditions were 94°C 15min, 22x (94°C 30sec, 57°C 3min, 72°C 1min), 68°C 30min. Multiplex PCR product were diluted in the PCR plate by adding 10 µL of water, and this diluted product was used as template for the Index-PCR. Index PCRs included 1x NEB Thermopol Reaction buffer (New England Biolabs, Whitby ON), 0.2mM dNTP, 0.2µM each indexing primer, 0.25U *Taq* DNA polymerase (NEB) and 0.5µL diluted template from the multiplex-PCR in a total volume of 5.0µL. Indexing primers were designed to contain the Illumina annealing adapter, allowing annealing of the PCR product to the flow cell and a unique 6-base index. Cycling conditions were 95°C 2min, 20x (95°C 20sec, 60°C 1min, 72°C 1min), 72°C 10min.

Index PCRs were pooled, quantified using a Kapa SYBR FAST qPCR kit (Kapa Biosystems Inc., Wilmington, MA) following the manufacturers recommended protocol on a Roche Lightcycler 480 qPCR instrument. The library was sequenced on an Illumina MiSeq DNA sequencer using a 150 cycle v3 sequencing kit (Illumina, San Diego CA).

Multilocus genotypes were determined from the sequence data using bioinformatic procedures and software described in Zhan et al. (in review). Four striped bass samples that had previously been genotyped with these microsatellite loci were used as positive controls to ensure comparability of genotypes obtained in this study with microsatellite genotypes previously obtained in the Marine Gene Probe Lab.

Multilocus microsatellite genotypes obtained in this study were analyzed together with existing multilocus data from 611 striped bass of known population origins (Shubenacadie/Stewiacke, $N = 258$; U.S. [Chesapeake Bay, Hudson River, Kennebec River], $N = 235$; Miramichi River, $N = 118$). Bayesian clustering using the program STRUCTURE 2.3.4 (Pritchard et al. 2000; Hubisz et al. 2009) was employed to assess the most likely population of origin for the striped bass in this study. Structure estimates the relative proportions (q) of each of k 'genetic clusters' in the genome of each individual. Individuals whose genetic background is entirely or primarily derived from a single population will typically have a q value approaching 1 for the proportion of their genome derived from the genetic cluster characteristic of that population. Based on the results of previous population genetic analyses of striped bass in Atlantic Canada (Bentzen *et al*. 2009; Bentzen unpublished data), analyses in this study were conducted assuming that k

= 3. STRUCTURE analyses were conducted using the correlated allele frequencies model, with 300,000 and 1,000,000 burn-in and randomizations, respectively. Analyses were conducted both with and without use of sample origins (location priors).

To further visualize the genetic data, a factorial correspondence analysis (FCA) was conducted using Genetix (Belkir *et al.* 1996-2004).

Results and Discussion

As shown in previous analyses (Bentzen et al. 2009, Bentzen unpublished data), Bayesian clustering of striped bass genotypes using Structure revealed clear genetic distinctions between three population groups of striped bass: **U.S.** (including Chesapeake Bay, Hudson River, and Kennebec River), Shubenacadie and Stewiacke River (henceforth, **Shu**), and Miramichi River (henceforth, **Mir**). The great majority of the striped bass analyzed in this study clustered strongly with the Shu population (Table 2; Figures 1,2). Of 294 striped bass genotyped for this study, 278 had *q* values > 0.90 for the **Shu** genetic cluster, strong evidence that they were members of that population. An additional 12 striped bass had *q* values in the range 0.78—0.89 for **Shu** population membership. Values of *q* in this range suggest some possibility of mixed population ancestry, but still point strongly to **Shu** being the immediate population of origin. Two striped bass had more intermediate *q* values (J1316-16G: 0.66 [**Shu**], 0.03 [**U.S.**], 0.30 [**Mir**]; S06676-20I: 0.63 [**Shu**], 0.25 [**U.S.**], 0.11 [**Mir**]) suggesting an even greater possibility of mixed population ancestry, but nonetheless, consistent with immediate origin of the fish in the **Shu** population. The one clear exception to the general pattern of membership in the **Shu** population was sample J0066-1D, which had *q* values of 0.01, 0.98, and 0.01 for **Shu**, **U.S**. and **Mir**, respectively. This result indicates that fish J0066-1D was almost certainly a migrant from a U.S. population.

An FCA plot depicting the relationships of the striped bass genotypes obtained in this study, relative to existing data for striped bass from the three reference populations is shown in Figure 2. The FCA plot shows that with the exception of one individual, the fish genotyped in this study are genetically similar to striped bass from the **Shu** reference collection.

References

Belkhir K, Borsa P, Chikhi ., Raufaste N and Bonhomme F. 1996-2004 GENETIX 4.05, logiciel sous Windows TM pour la génétique des populations. Laboratoire Génome, Populations, Interactions, CNRS UMR 5000, Université de Montpellier II, Montpellier (France).

Bentzen P, Paterson IG, and Bradford RG. 2009. Greater genetic differentiation and complex migratory behavior of striped bass in the Canadian Portion of the species range. p.923. *American Fisheries Society Symposium* 69.

Bradford RG, LeBlanc P, and Bentzen P. 2012. Update Status Report on Bay of Fundy Striped Bass (*Morone saxatilis*). *DFO Can. Sci. Advis. Sec. Sci. Res. Doc. Rep*. 2012/021: vi + 46p

Brown KM, Baltazar GA, Weinstein BN, Hamilton MB. 2003. Isolation and characterization of nuclear microsatellite loci in the anadromous marine fish *Morone saxatilis. Molecular Ecology Notes* **3,** 414–416

COSEWIC. 2012. COSEWIC assessment and status report on the Striped Bass Morone saxatilis in Canada. Committee on the Status of Endangered Wildlife in Canada. Ottawa. Iv + 82pp. (www.registrelep-sararegistry.gc.ca/default_e.cfm).

Elphinstone MS, Hinten GN, Anderson MJ, Nock CJ. 2003. An inexpensive and high-throughput procedure to extract and purify total genomic DNA for population studies *Molecular Ecology Notes*, **3**, 317-320.

Hubisz MJ, Falush D, Stephens M, and Pritchard JK. 2009. Inferring weak population structure with assistance of sample group information. *Molecular Ecology Resources* **9(5)**, 1322-1332.

Pritchard JK, Stephens M, Donnelly P. 2000. Inference of population structure using multilocus genotype data. *Genetics*, **155**, 945-959.

Rexroad C, Vellejo R, Coulibaly, I, Couch, C, Garber A, Westerman M, Sullivan C. 2006. Identification and characterization of microsatellites for striped bass from repeat-enriched libraries. *Conservation Genetics* 7, 971–982.

Ross K, Wang X, O'Malley KG, Gatlin DMIII, GOLD JR. 2004. Microsatellite DNA markers for parental assignment in hybrid striped bass (*Morone saxatilis*×*Morone chrysops*). Molecular Ecology Notes **4,** 156–159

Roy NK, Maceda L, Wirgin I. 2000. Isolation of microsatellites in striped bass *Morone saxatilis* (Teleostei) and their preliminary use in population identification. *Molecular Ecology* **9,** 827–829

Zhan L, Paterson IG, Fraser BA, Watson B, Bradbury IR, Nadukkalan Pravindran P, Reznick D, Beiko RG, Bentzen P. MEGASAT: automated inference of microsatellite genotypes from sequence data. *Molecular Ecology Resources* (in review).

Table 1. Microsatellite loci and primers used in this study.

Locus[1]	Repeat Motif	Accession #[2]	Primers (F over R)[3]	Size range (b)[4]	Tailed version of primers[5]	Reference[6]
Msm1592	TAGA	BV678609	AGTTACTCAGGATATGTTAGTTGG TTCCCTCGGGATGAATAAAG	100-244	CCCTACACGACGCTCTTCCGATCTAGTTACTCAGGATATGTTAGTTGG GTTCAGACGTGTGCTCTTCCGATCTTTCCCTCGGGATGAATAAAG	A
Msm1628	TAGA	BV678636	ATCCCACATGGAGTTGTAG TGTTGCAGTGTATGTATTGAATG	84-164	CCCTACACGACGCTCTTCCGATCTATCCCACATGGAGTTGTAG GTTCAGACGTGTGCTCTTCCGATCTTGTTGCAGTGTATGTATTGAATG	A
Msm1604	ATCT	BV678618	ACCGCTGGAAACTGTGAATC AACACACCTTGTGAGGCAGA	82-210	CCCTACACGACGCTCTTCCGATCTACCGCTGGAAACTGTGAATC GTTCAGACGTGTGCTCTTCCGATCTAACACACCTTGTGAGGCAGA	A
Msm1625	ATCT	BV678633	AAGCTTCCATATAGTGCACCC TCGCTGCTTACACCACTCAG	141-213	CCCTACACGACGCTCTTCCGATCTAAGCTTCCATATAGTGCACCC GTTCAGACGTGTGCTCTTCCGATCTTCGCTGCTTACACCACTCAG	A
Msm1357	GATA	BV678321	CCTTCCTGCCAGTCCATACT CAATTAAGCAGCCCGACTCT	121-189	CCCTACACGACGCTCTTCCGATCTCCTTCCTGCCAGTCCATACT GTTCAGACGTGTGCTCTTCCGATCTCAATTAAGCAGCCCGACTCT	A
Msm1584	ATCT	BV678601	TGGGGTGAGGACACTGAGTT AAGGACAGCCAATCAGAGGA	88-160	CCCTACACGACGCTCTTCCGATCTTGGGGTGAGGACACTGAGTT GTTCAGACGTGTGCTCTTCCGATCTAAGGACAGCCAATCAGAGGA	A
Msm1645	CTAT	BV678651	GATGCAGAAGTATGGTACTGAGACA AAATGCAACCTGTGCTGATA	86-162	CCCTACACGACGCTCTTCCGATCTGATGCAGAAGTATGGTACTGAGACA GTTCAGACGTGTGCTCTTCCGATCTAAATGCAACCTGTGCTGATA	A
MsaAT150-2#4 (Msa8)	GT	AY248732	GCCATGTGTTGGCACATTTA TGTCAAGGGATTGAAACACTTTT	83-117	CCCTACACGACGCTCTTCCGATCTGCCATGTGTTGGCACATTTA GTTCAGACGTGTGCTCTTCCGATCTTGTCAAGGGATTGAAACACTTTT	B

MsaAG25-1 (Msa4)	CTTT	AY248735	TGTAATTTATATTATTTCGTGTTGTGC ATCCTGCCTGCTGTATTTGG	92-268	CCCTACACGACGCTCTTCCGATCTTGTAATTTATATTATTTCGTGTTGTGC GTTCAGACGTGTGCTCTTCCGATCTATCCTGCCTGCTGTATTTGG	B
MsaAC25-6 (Msa1)	TG	AY248734	TGGTCCAATCATGGGTTTATG AAAACAATTGATACGCTCAGTCT	88-136	CCCTACACGACGCTCTTCCGATCTTGGTCCAATCATGGGTTTATG GTTCAGACGTGTGCTCTTCCGATCTAAAACAATTGATACGCTCAGTCT	B
Hsb1B	GT	AY453797	CAGCAGAAGTTGGGACTGGTA TTCCCCATTCCCCCTTT	98-150	CCCTACACGACGCTCTTCCGATCTCAGCAGAAGTTGGGACTGGTA GTTCAGACGTGTGCTCTTCCGATCTTTCCCCATTCCCCCTTT	C

1: For loci with two names, the one given in parentheses is the one used in this report.

2: Genbank

3: Primers used in this study were redesigned from those given in reference publications.

4: Size range of microsatellite amplicons observed in this study.

5: Sequences of primers including 'tails' added to enable sequencing on Illumina DNA sequencer

6: A, Rexroad *et al*. 2006; B, Brown *et al*. 2003; C, Ross *et al*. 2004.

Figure 1. Bar plot showing results of Bayesian clustering of striped bass using Structure. The colours represent the estimated proportional ancestry of each individual (blue, Shubenacadie/Stewiacke; red, U.S.; yellow, Miramichi). Panels A-C show individuals included in this analysis. Panel D also includes individuals from this study (samples SO6568-19C -- SO6678-20K) as well as representative individuals from U.S. populations (Chesapeake, Hudson River, Kennebec River; samples Ch16 -- Ke05), Shubenacadie/Stewiacke (samples Sh08 -- Sh19) and Miramichi River (samples MirSB95498 -- MirSB00015). Note that sample J0066-1D shows strong evidence of U.S. ancestry. Individual J0811-8I may be of mixed Shubenacadie/U.S. ancestry.

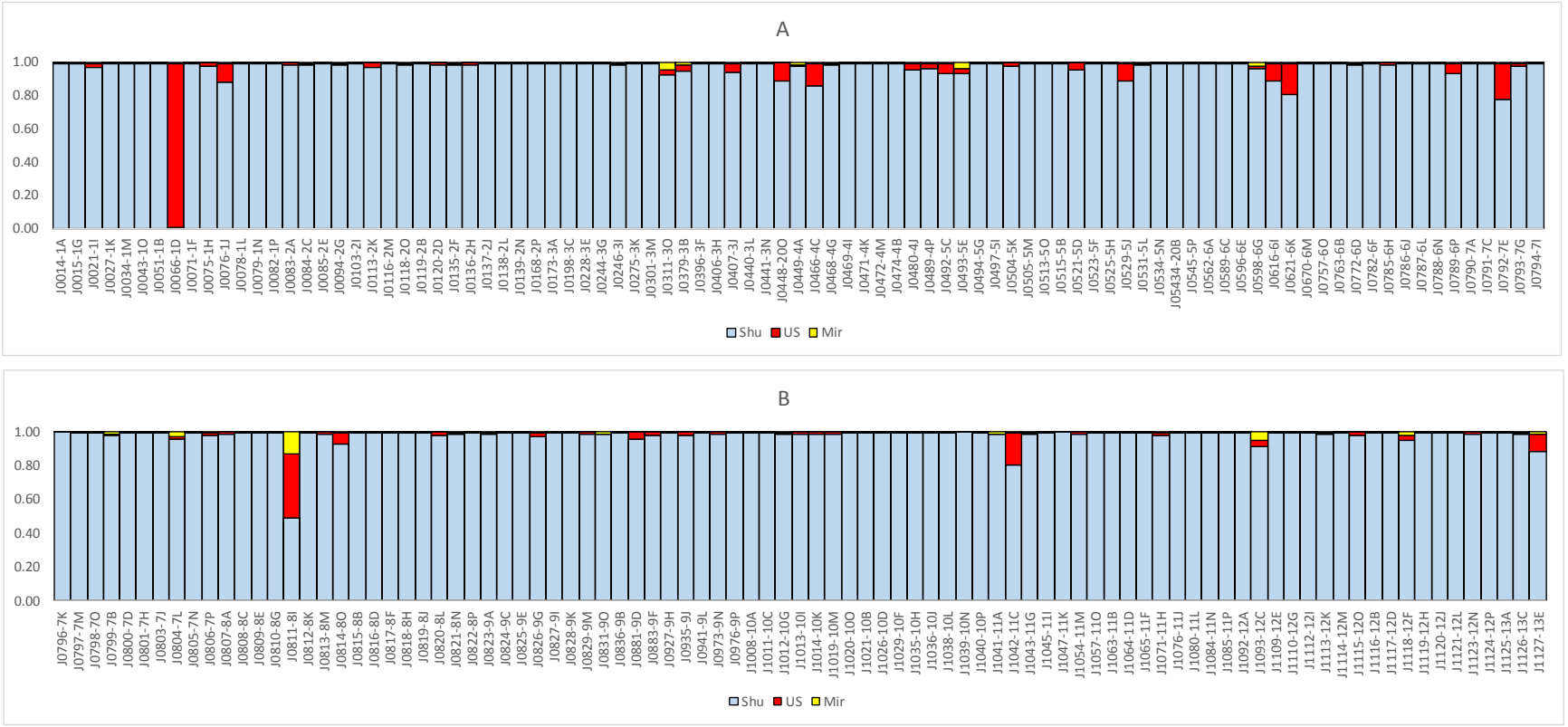

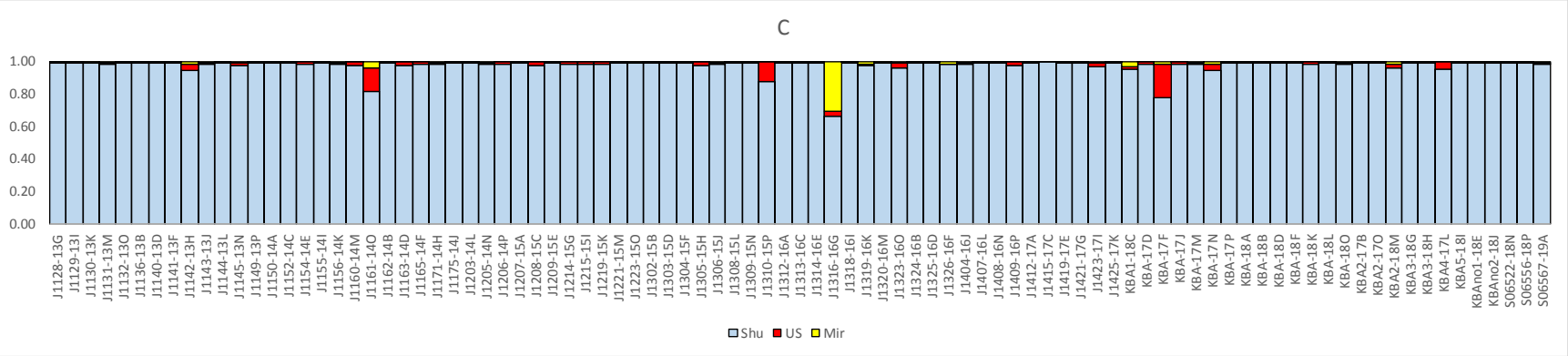
C
1.00
0.80
0.60
0.40
0.20
0.00
J1128-13G
J1129-13I
J1130-13K
J1131-13M
J1132-13O
J1136-13B
J1140-13D
J1141-13F
J1142-13H
J1143-13J
J1144-13L
J1145-13N
J1149-13P
J1150-14A
J1152-14C
J1154-14E
J1155-14I
J1156-14K
J1160-14M
J1161-14O
J1162-14B
J1163-14D
J1165-14F
J1171-14H
J1175-14J
J1203-14L
J1205-14N
J1206-14P
J1207-15A
J1208-15C
J1209-15E
J1214-15G
J1215-15I
J1219-15K
J1221-15M
J1223-15O
J1302-15B
J1303-15D
J1304-15F
J1305-15H
J1306-15J
J1308-15L
J1309-15N
J1310-15P
J1312-16A
J1313-16C
J1314-16E
J1316-16G
J1318-16I
J1319-16K
J1320-16M
J1323-16O
J1324-16B
J1325-16D
J1326-16F
J1404-16J
J1407-16L
J1408-16N
J1409-16P
J1412-17A
J1415-17C
J1419-17E
J1421-17G
J1423-17I
J1425-17K
KBA1-18C
KBA-17D
KBA-17F
KBA-17J
KBA-17M
KBA-17N
KBA-17P
KBA-18A
KBA-18B
KBA-18D
KBA-18F
KBA-18K
KBA-18L
KBA-18O
KBA2-17B
KBA2-17O
KBA2-18M
KBA3-18G
KBA3-18H
KBA4-17L
KBA5-18I
KBAno1-18E
KBAno2-18J
S06522-18N
S06556-18P
S06567-19A
Shu
US
Mir

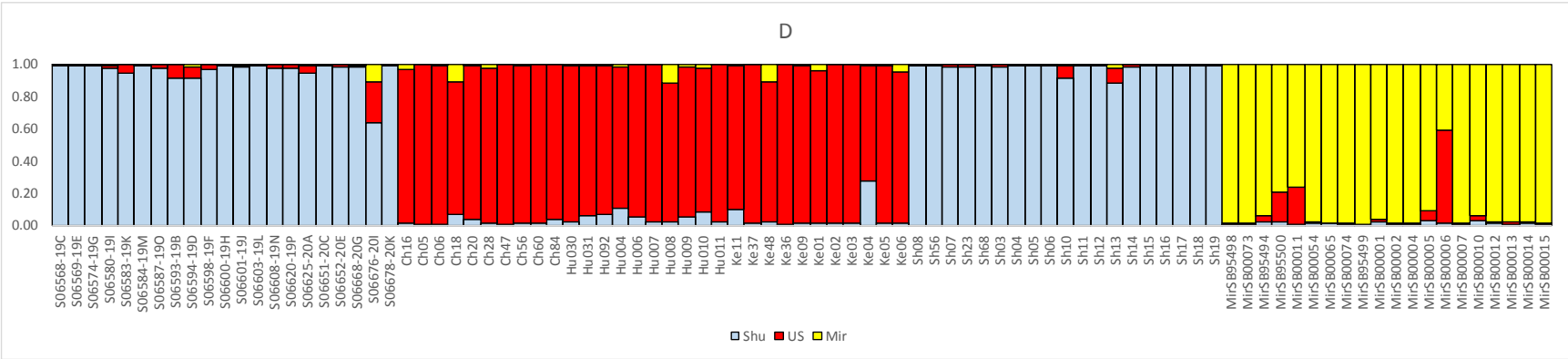
D
1.00
0.80
0.60
0.40
0.20
0.00
S06568-19C
S06569-19E
S06574-19G
S06580-19I
S06583-19K
S06584-19M
S06587-19O
S06593-19B
S06594-19D
S06598-19F
S06600-19H
S06601-19J
S06603-19L
S06608-19N
S06620-19P
S06625-20A
S06651-20C
S06652-20E
S06668-20G
S06676-20I
S06678-20K
Ch16
Ch05
Ch06
Ch18
Ch20
Ch28
Ch47
Ch56
Ch60
Ch84
Hu030
Hu031
Hu092
Hu004
Hu006
Hu007
Hu008
Hu009
Hu010
Hu011
Ke11
Ke37
Ke48
Ke36
Ke09
Ke01
Ke02
Ke03
Ke04
Ke05
Ke06
Sh08
Sh56
Sh07
Sh23
Sh68
Sh03
Sh04
Sh05
Sh06
Sh10
Sh11
Sh12
Sh13
Sh14
Sh15
Sh16
Sh17
Sh18
Sh19
MirSB95498
MirSB00073
MirSB95494
MirSB95500
MirSB00011
MirSB00054
MirSB00065
MirSB00074
MirSB95499
MirSB00001
MirSB00002
MirSB00004
MirSB00005
MirSB00006
MirSB00007
MirSB00010
MirSB00012
MirSB00013
MirSB00014
MirSB00015
Shu
US
Mir

Figure 2. Factorial correspondence plot showing genetic relationships of individual striped bass. Yellow, samples from this study; white, Shubenacadie/Stewiacke population; blue, U.S. population; grey, Miramichi population.

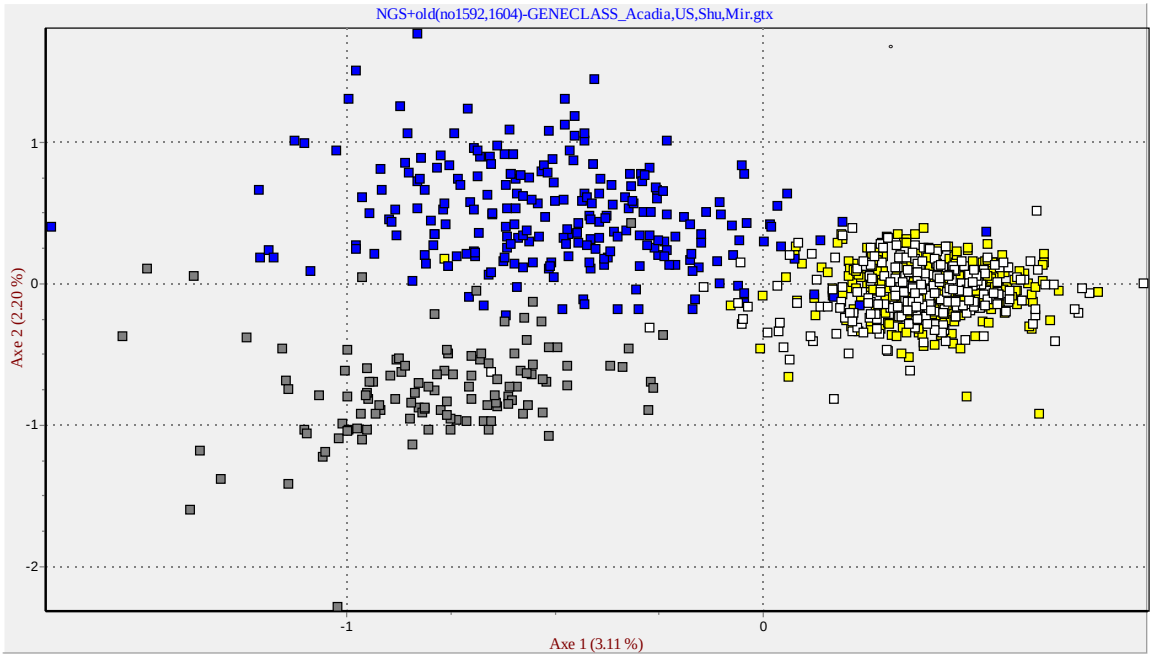

Appendix 1. List of striped bass samples successfully genotyped in this study, and their ancestry coefficients ('q values') for three potential source populations: Shu, U.S., Mir.

ID	Shu	U .S.	Mir
J0014-1A	0.99	0.01	0.00
J0015-1G	0.99	0.01	0.01
J0021-1I	0.97	0.02	0.01
J0027-1K	0.99	0.01	0.00
J0034-1M	0.99	0.00	0.00
J0043-1O	0.99	0.00	0.00
J0051-1B	0.99	0.00	0.00
J0066-1D	0.01	0.98	0.01
J0071-1F	0.99	0.00	0.00
J0075-1H	0.98	0.02	0.00
J0076-1J	0.88	0.12	0.01
J0078-1L	0.99	0.00	0.00
J0079-1N	0.99	0.01	0.00
J0082-1P	0.99	0.00	0.00
J0083-2A	0.99	0.01	0.00
J0084-2C	0.99	0.01	0.01
J0085-2E	0.99	0.01	0.00
J0094-2G	0.99	0.01	0.01
J0103-2I	0.99	0.01	0.00
J0113-2K	0.97	0.02	0.00
J0116-2M	0.99	0.00	0.00
J0118-2O	0.98	0.01	0.00
J0119-2B	0.99	0.01	0.00
J0120-2D	0.99	0.01	0.00
J0135-2F	0.99	0.00	0.01
J0136-2H	0.98	0.01	0.00
J0137-2J	0.99	0.01	0.00
J0138-2L	0.99	0.00	0.00
J0139-2N	0.99	0.01	0.00
J0168-2P	0.99	0.01	0.00
J0173-3A	0.99	0.00	0.00
J0198-3C	0.99	0.01	0.00
J0228-3E	0.99	0.01	0.00
J0244-3G	0.99	0.00	0.00
J0246-3I	0.99	0.01	0.01
J0275-3K	0.99	0.01	0.00
J0301-3M	0.99	0.00	0.00
J0311-3O	0.92	0.03	0.05
J0379-3B	0.95	0.04	0.01

J0396-3F	0.99	0.00	0.00
J0406-3H	1.00	0.00	0.00
J0407-3J	0.94	0.06	0.00
J0440-3L	0.99	0.00	0.00
J0441-3N	0.99	0.00	0.00
J0448-20O	0.89	0.10	0.00
J0449-4A	0.98	0.00	0.01
J0466-4C	0.86	0.13	0.01
J0468-4G	0.98	0.01	0.01
J0469-4I	0.99	0.01	0.00
J0471-4K	0.99	0.00	0.00
J0472-4M	0.99	0.01	0.00
J0474-4B	0.99	0.01	0.00
J0480-4J	0.96	0.04	0.01
J0489-4P	0.97	0.02	0.01
J0492-5C	0.94	0.06	0.01
J0493-5E	0.93	0.04	0.03
J0494-5G	0.99	0.00	0.00
J0497-5I	0.99	0.01	0.00
J0504-5K	0.98	0.02	0.00
J0505-5M	0.99	0.00	0.00
J0513-5O	0.99	0.01	0.00
J0515-5B	0.99	0.00	0.00
J0521-5D	0.96	0.04	0.00
J0523-5F	0.99	0.00	0.00
J0525-5H	0.99	0.00	0.00
J0529-5J	0.89	0.10	0.01
J0531-5L	0.99	0.01	0.00
J0534-5N	0.99	0.00	0.00
J05434-20B	0.99	0.00	0.00
J0545-5P	0.99	0.00	0.00
J0562-6A	0.99	0.00	0.00
J0589-6C	0.99	0.00	0.01
J0596-6E	0.99	0.01	0.00
J0598-6G	0.97	0.01	0.02
J0616-6I	0.89	0.10	0.01
J0621-6K	0.80	0.19	0.01
J0670-6M	0.99	0.01	0.00
J0757-6O	0.99	0.01	0.00
J0763-6B	0.99	0.01	0.00
J0772-6D	0.98	0.01	0.01
J0782-6F	0.99	0.01	0.00
J0785-6H	0.99	0.01	0.00

J0786-6J	0.99	0.00	0.00
J0787-6L	0.99	0.00	0.00
J0788-6N	0.99	0.00	0.00
J0789-6P	0.93	0.06	0.01
J0790-7A	0.99	0.00	0.00
J0791-7C	0.99	0.01	0.01
J0792-7E	0.78	0.22	0.00
J0793-7G	0.98	0.01	0.01
J0794-7I	0.99	0.00	0.00
J0796-7K	1.00	0.00	0.00
J0797-7M	0.99	0.01	0.00
J0798-7O	0.99	0.00	0.01
J0799-7B	0.98	0.01	0.01
J0800-7D	0.99	0.01	0.01
J0801-7H	0.99	0.00	0.00
J0803-7J	0.99	0.00	0.00
J0804-7L	0.95	0.01	0.03
J0805-7N	0.99	0.00	0.01
J0806-7P	0.98	0.01	0.01
J0807-8A	0.99	0.01	0.00
J0808-8C	0.99	0.00	0.00
J0809-8E	0.99	0.00	0.01
J0810-8G	0.99	0.00	0.00
J0811-8I	0.49	0.38	0.13
J0812-8K	0.99	0.01	0.00
J0813-8M	0.98	0.02	0.00
J0814-8O	0.92	0.07	0.01
J0815-8B	0.99	0.01	0.00
J0816-8D	0.99	0.00	0.00
J0817-8F	0.99	0.00	0.00
J0818-8H	0.99	0.00	0.00
J0819-8J	0.99	0.01	0.00
J0820-8L	0.98	0.02	0.00
J0821-8N	0.98	0.01	0.01
J0822-8P	0.99	0.00	0.01
J0823-9A	0.98	0.01	0.01
J0824-9C	0.99	0.00	0.00
J0825-9E	0.99	0.00	0.00
J0826-9G	0.97	0.03	0.01
J0827-9I	0.99	0.00	0.01
J0828-9K	0.99	0.00	0.00
J0829-9M	0.99	0.01	0.00
J0831-9O	0.98	0.00	0.01

J0836-9B	0.99	0.00	0.00
J0881-9D	0.95	0.04	0.00
J0883-9F	0.98	0.02	0.00
J0927-9H	0.99	0.00	0.00
J0935-9J	0.97	0.02	0.00
J0941-9L	0.99	0.00	0.00
J0973-9N	0.99	0.01	0.00
J0976-9P	0.99	0.01	0.00
J1008-10A	0.99	0.00	0.00
J1011-10C	0.99	0.00	0.00
J1012-10G	0.98	0.01	0.01
J1013-10I	0.99	0.01	0.00
J1014-10K	0.99	0.01	0.00
J1019-10M	0.99	0.01	0.00
J1020-10O	0.99	0.01	0.00
J1021-10B	0.99	0.00	0.00
J1026-10D	0.99	0.00	0.00
J1029-10F	0.99	0.00	0.00
J1035-10H	0.99	0.00	0.00
J1036-10J	0.99	0.00	0.00
J1038-10L	0.99	0.00	0.01
J1039-10N	1.00	0.00	0.00
J1040-10P	0.99	0.01	0.00
J1041-11A	0.98	0.00	0.01
J1042-11C	0.80	0.19	0.01
J1043-11G	0.99	0.01	0.01
J1045-11I	0.99	0.00	0.00
J1047-11K	1.00	0.00	0.00
J1054-11M	0.98	0.02	0.00
J1057-11O	0.99	0.01	0.00
J1063-11B	0.99	0.01	0.00
J1064-11D	0.99	0.01	0.00
J1065-11F	0.99	0.01	0.00
J1071-11H	0.98	0.01	0.01
J1076-11J	0.99	0.01	0.00
J1080-11L	0.99	0.00	0.00
J1084-11N	0.99	0.01	0.00
J1085-11P	0.99	0.00	0.00
J1092-12A	0.99	0.01	0.00
J1093-12C	0.91	0.03	0.05
J1109-12E	0.99	0.00	0.00
J1110-12G	0.99	0.01	0.00
J1112-12I	0.99	0.01	0.00

J1113-12K	0.99	0.01	0.01
J1114-12M	0.99	0.00	0.00
J1115-12O	0.97	0.02	0.00
J1116-12B	0.99	0.01	0.00
J1117-12D	0.99	0.00	0.00
J1118-12F	0.95	0.03	0.02
J1119-12H	0.99	0.00	0.00
J1120-12J	0.99	0.00	0.00
J1121-12L	0.99	0.01	0.00
J1123-12N	0.99	0.01	0.00
J1124-12P	0.99	0.00	0.00
J1125-13A	0.99	0.00	0.00
J1126-13C	0.98	0.01	0.01
J1127-13E	0.88	0.10	0.02
J1128-13G	0.99	0.01	0.00
J1129-13I	0.99	0.00	0.00
J1130-13K	0.99	0.00	0.01
J1131-13M	0.99	0.01	0.01
J1132-13O	0.99	0.00	0.00
J1136-13B	0.99	0.01	0.00
J1140-13D	0.99	0.00	0.00
J1141-13F	0.99	0.00	0.00
J1142-13H	0.94	0.04	0.02
J1143-13J	0.98	0.01	0.01
J1144-13L	0.99	0.00	0.00
J1145-13N	0.98	0.02	0.01
J1149-13P	0.99	0.01	0.00
J1150-14A	0.99	0.00	0.00
J1152-14C	0.99	0.00	0.00
J1154-14E	0.99	0.01	0.00
J1155-14I	0.99	0.00	0.00
J1156-14K	0.98	0.01	0.01
J1160-14M	0.98	0.02	0.00
J1161-14O	0.82	0.14	0.04
J1162-14B	0.99	0.00	0.00
J1163-14D	0.98	0.02	0.00
J1165-14F	0.99	0.01	0.01
J1171-14H	0.98	0.01	0.01
J1175-14J	0.99	0.01	0.00
J1203-14L	0.99	0.01	0.00
J1205-14N	0.98	0.00	0.01
J1206-14P	0.99	0.01	0.00
J1207-15A	0.99	0.00	0.00

J1208-15C	0.98	0.02	0.00
J1209-15E	0.99	0.00	0.00
J1214-15G	0.98	0.01	0.00
J1215-15I	0.99	0.01	0.00
J1219-15K	0.98	0.02	0.00
J1221-15M	0.99	0.01	0.00
J1223-15O	0.99	0.01	0.01
J1302-15B	0.99	0.00	0.00
J1303-15D	0.99	0.01	0.00
J1304-15F	0.99	0.00	0.00
J1305-15H	0.98	0.02	0.00
J1306-15J	0.98	0.01	0.01
J1308-15L	0.99	0.01	0.00
J1309-15N	0.99	0.01	0.00
J1310-15P	0.88	0.12	0.01
J1312-16A	0.99	0.00	0.00
J1313-16C	0.99	0.00	0.00
J1314-16E	0.99	0.00	0.00
J1316-16G	0.66	0.03	0.30
J1318-16I	0.99	0.01	0.00
J1319-16K	0.98	0.01	0.02
J1320-16M	0.99	0.00	0.01
J1323-16O	0.96	0.03	0.01
J1324-16B	0.99	0.01	0.00
J1325-16D	0.99	0.00	0.00
J1326-16F	0.98	0.00	0.01
J1404-16J	0.99	0.01	0.01
J1407-16L	0.99	0.00	0.00
J1408-16N	0.99	0.01	0.00
J1409-16P	0.97	0.03	0.00
J1412-17A	0.99	0.01	0.00
J1415-17C	1.00	0.00	0.00
J1419-17E	0.99	0.00	0.00
J1421-17G	0.99	0.00	0.00
J1423-17I	0.97	0.02	0.01
J1425-17K	0.99	0.01	0.00
KBA1-18C	0.95	0.02	0.03
KBA-17D	0.98	0.02	0.00
KBA-17F	0.78	0.20	0.02
KBA-17J	0.98	0.01	0.00
KBA-17M	0.98	0.01	0.01
KBA-17N	0.95	0.03	0.02
KBA-17P	0.99	0.01	0.00

KBA-18A	0.99	0.00	0.00
KBA-18B	0.99	0.00	0.01
KBA-18D	0.99	0.01	0.00
KBA-18F	0.99	0.01	0.00
KBA-18K	0.98	0.01	0.00
KBA-18L	0.99	0.00	0.00
KBA-18O	0.98	0.01	0.01
KBA2-17B	0.99	0.01	0.00
KBA2-17O	0.99	0.01	0.00
KBA2-18M	0.96	0.02	0.02
KBA3-18G	0.99	0.01	0.00
KBA3-18H	0.99	0.01	0.00
KBA4-17L	0.95	0.04	0.00
KBA5-18I	0.99	0.01	0.00
KBAno1-18E	0.99	0.01	0.00
KBAno2-18J	0.99	0.00	0.00
S06522-18N	0.99	0.00	0.00
S06556-18P	0.99	0.00	0.01
S06567-19A	0.99	0.00	0.01
S06568-19C	0.99	0.01	0.00
S06569-19E	0.99	0.01	0.00
S06574-19G	0.99	0.01	0.00
S06580-19I	0.97	0.02	0.01
S06583-19K	0.95	0.05	0.00
S06584-19M	0.99	0.01	0.00
S06587-19O	0.98	0.02	0.00
S06593-19B	0.91	0.08	0.00
S06594-19D	0.91	0.07	0.02
S06598-19F	0.97	0.03	0.00
S06600-19H	0.99	0.00	0.00
S06601-19J	0.99	0.01	0.01
S06603-19L	0.99	0.00	0.00
S06608-19N	0.98	0.02	0.00
S06620-19P	0.98	0.02	0.00
S06625-20A	0.95	0.05	0.01
S06651-20C	0.99	0.00	0.01
S06652-20E	0.99	0.01	0.00
S06668-20G	0.99	0.01	0.01
S06676-20I	0.63	0.25	0.11
S06678-20K	0.99	0.01	0.00